Available online at www.sciencedirect.com
SCIENCE DIRECT®
Appl. Comput. Harmon. Anal. 19 (2005) 223–252
Applied and Computational Harmonic Analysis
www.elsevier.com/locate/acha

Stereographic wavelet frames on the sphere

I. Bogdanova [a], P. Vandergheynst [a], J-P. Antoine [b,*], L. Jacques [b], M. Morvidone [b,1]

[a] *Signal Processing Institute (ITS), School of Engineering (STI), Swiss Federal Institute of Technology (EPFL), CH-1015 Lausanne, Switzerland*

[b] *Institut de Physique Théorique, Université Catholique de Louvain, B-1348 Louvain-la-Neuve, Belgium*

Received 5 October 2004; revised 30 April 2005; accepted 20 May 2005

Available online 20 July 2005

Communicated by Bruno Torresani

Abstract

In this paper we exploit the continuous wavelet transform (CWT) on the two-dimensional sphere S^2, introduced previously by two of us, to build associated discrete wavelet frames. We first explore half-continuous frames, i.e., frames where the position remains a continuous variable, and then move on to a fully discrete theory. We introduce the notion of controlled frames, which reflects the particular nature of the underlying theory, in particular the apparent conflict between dilation and the compactness of the S^2 manifold. We also highlight some implementation issues and provide numerical illustrations.

Keywords: Continuous wavelet transform; Spherical wavelets; Discrete wavelet frames; Half-continuous frames; Controlled frames

1. Introduction

Many situations in physics and medicine require the existence of suitable tools for analyzing data on spherical manifolds. In that case, as usual, the Fourier transform (FT) is a standard tool, which amounts to an expansion in spherical harmonics, whose support is the whole sphere. The Fourier series on S^2 is thus

* Corresponding author.
E-mail addresses: iva.bogdanova@epfl.ch (I. Bogdanova), pierre.vandergheynst@epfl.ch (P. Vandergheynst), antoine@fyma.ucl.ac.be (J-P. Antoine), ljacques@fyma.ucl.ac.be (L. Jacques), mmorvido@math.unl.edu.ar (M. Morvidone).
[1] Present address: IMAL, 3000 Santa Fe, Argentina.

1063-5203/$ – see front matter
doi:10.1016/j.acha.2005.05.001

global and somewhat cumbersome. It turns out that, as an analysis tool, the continuous wavelet transform (CWT) has many advantages over the FT. In particular, the spherical CWT is local and is controlled by two intuitive operations: dilation and transport over the sphere by rotations.

Thus, quite naturally, many authors have tried to design a suitable spherical CWT, for instance, Torrésani [28], Rubin [25,26], or Holschneider [16]. However, none of the resulting tools is completely satisfactory. At last, a rigorous, yet efficient transform was developed by several of us, in two successive papers [4,5]. The technique is grounded in group theory, more precisely the coherent state approach based on square integrable group representations [3]. The relevant group here is the conformal group of the two-sphere S^2, namely, the Lorentz group $\mathrm{SO}_o(1,3)$. The upshot of these two papers is a rigorous spherical CWT, together with a detailed analysis of its numerical implementation, including a suitable discretization scheme.

The present paper is a continuation of [4,5] and improves on them in two respects. First, we present a detailed construction of *frames* associated to the spherical CWT. These actually come in various flavors. Besides the usual discrete frames [11], semi-continuous frames[2] and the continuous frames familiar in coherent state theory [3], we also introduce *controlled* and *weighted* frames, which are a natural generalization of plain frames. In addition, we also propose an efficient implementation through a systematic use of the fast spherical convolution introduced by Driscoll and Healy [12]. The resulting tool is quite efficient, as illustrated by several examples [21,31,32]. It opens interesting perspectives for practical applications in a number of fields, such as geophysics, astronomy and astrophysics, light field processing [9], omnidirectional vision [31,32] and medical imaging (e.g., EEG, the sphere being a good approximation of the skull).

The paper is organized as follows. We begin by reviewing in Section 2 the general theory of the CWT on the two-sphere and its practical implementation. We basically follow [4,5], with particular emphasis on the determination of the range of the scale parameter. As a general reference on 2-D wavelets, we use our recent monograph [7]. Then, in Section 3, we discuss the various notions of abstract frames, discrete, continuous and half-continuous, as well as a useful generalization of the standard concept, called a controlled frame. Section 4 is the core of the paper. Here we derive, by two different methods, a class of half-continuous frames of spherical wavelets. We then turn to the case of fully discrete spherical frames. Finally, numerical examples are provided to illustrate the potential of these new frames.

2. The continuous wavelet transform on the 2-sphere

2.1. The general theory

The spherical CWT, as its Euclidean counterpart, is based on affine transformations. On the 2-dimensional sphere S^2, embedded in $\mathbb{R}^3$, the latter consist of rotations, defined by elements ρ of the group SO(3), and dilations, parameterized by the scale $a \in \mathbb{R}_+^*$ [4]. Let $L^2(S^2, \mathrm{d}\mu)$ be the space of finite energy signals on the sphere, that is, the Hilbert space of square integrable functions on S^2, with the rotation invariant Lebesgue measure $\mathrm{d}\mu(\theta, \varphi) = \sin\theta \, \mathrm{d}\theta \, \mathrm{d}\varphi$. In that space, the basic operations we consider are represented by the following unitary operators:

[2] Semi-continuous wavelet frames are also known as *Dyadic Wavelet Transforms* [19].

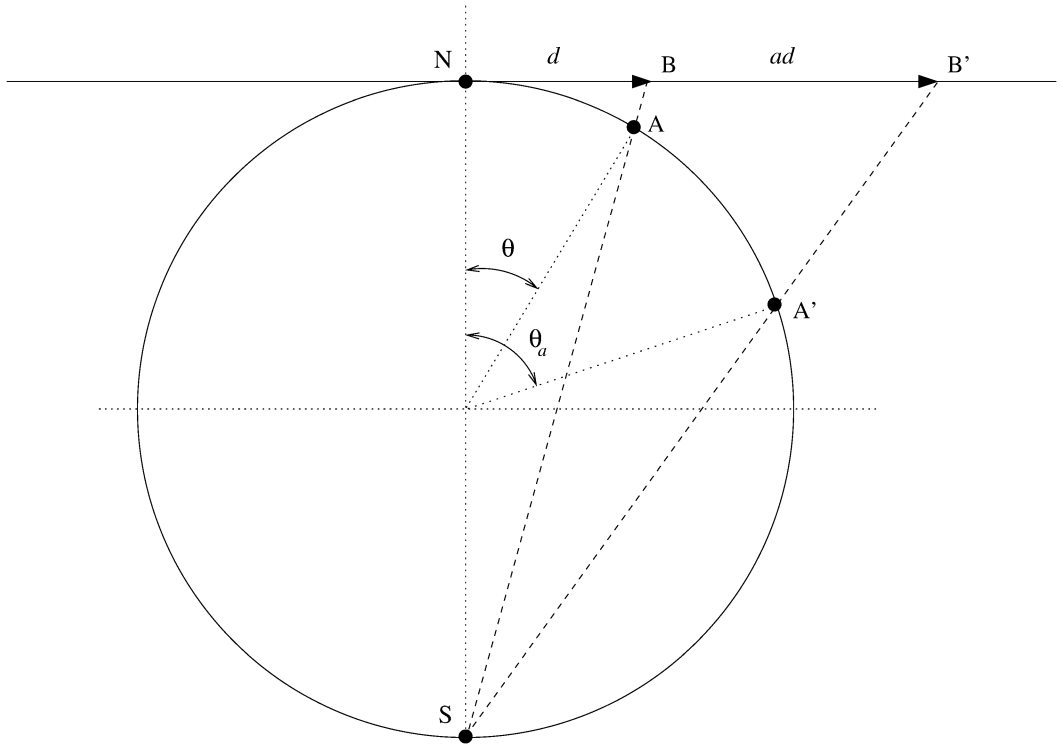

Fig. 1. Visual meaning of the stereographic dilation on S^2.

- rotation R_ρ, where $\rho \in \mathrm{SO}(3)$ may be parametrized in terms of its Euler angles:

$$(R_\rho f)(\omega) = f\left(\rho^{-1}\omega\right), \quad \omega \equiv (\theta, \varphi). \tag{2.1}$$

  In this equation, ρ is a 3×3 rotation matrix acting on a unit vector in $\mathbb{R}^3$.
- dilation D_a, with $a \in \mathbb{R}_+^*$:

$$(D_a f)(\omega) = \lambda(a, \theta)^{1/2} f(\omega_{1/a}), \tag{2.2}$$

  where $\omega_a \equiv (\theta_a, \varphi)$ with $\tan\frac{\theta_a}{2} = a \tan\frac{\theta}{2}$; $a > 0$, $\theta \in [0, \pi]$, $\varphi \in [0, 2\pi)$; and λ is a normalization factor. Technically, this factor is a cocycle or a Radon–Nikodým derivative, resulting from the fact that the Lebesgue measure μ is not invariant under dilations. It is given by

$$\lambda(a, \theta) = \frac{4a^2}{[(a^2 - 1)\cos\theta + (a^2 + 1)]^2}. \tag{2.3}$$

Intuitively, the action of the dilation D_a on a function $f \in L^2(S^2)$ may be understood as follows: project f on the plane tangent at the North Pole by a stereographic projection from the South Pole, apply a Euclidean dilation by a to the projection and lift the resulting function back to the sphere by inverse stereographic projection. Figure 1 illustrates this process by determining the image $A' \in S^2$ of a point $A \in S^2$ under dilation D_a.

In the language of group theory, these two affine transformations, which do not generate a group nor commute, belong to the conformal group of the sphere S^2—the Lorentz group $\mathrm{SO}_o(3,1)$—each subgroup

being one component in the Iwasawa decomposition (see [4] for details). Using these definitions, a square integrable function ψ on S^2 is called an *admissible wavelet* if and only if there is a finite constant $c \in \mathbb{R}_+^*$, such that for all $l \in \mathbb{N}$,

$$G_\psi(l) = \frac{8\pi^2}{2l+1} \sum_{|m|\leqslant l} \int_{\mathbb{R}_+^*} \frac{\mathrm{d}a}{a^3} \left|\hat{\psi}_a(l,m)\right|^2 < c, \tag{2.4}$$

where $\hat{\psi}_a(l,m) = \langle Y_l^m | \psi_a \rangle$ is the Fourier coefficient of $\psi_a = D_a \psi$. Note that the existence of (a dense set of) admissible vectors expresses the fact that the underlying representation of $\mathrm{SO}_o(3,1)$ is square integrable [4].

Fortunately, there exists a simpler requirement, nearly equivalent to (2.4) (strictly speaking, the condition is only sufficient), which consists in imposing

$$\int_{S^2} \mathrm{d}\mu(\theta,\varphi) \frac{\psi(\theta,\varphi)}{1+\cos\theta} = 0. \tag{2.5}$$

It has been shown in [4,5] that any admissible 2-D wavelet in $\mathbb{R}^2$ yields, by inverse stereographic projection, a spherical wavelet that satisfies (2.5).[3] In particular, for

$$\phi(\theta,\varphi) = \exp\left(-\tan^2\left(\frac{\theta}{2}\right)\right), \tag{2.6}$$

which is the inverse stereographic projection on the sphere of a Gaussian, a simple example of admissible wavelet is the *Difference of Gaussians* (DOG) spherical wavelet

$$\psi(\theta,\varphi) = \phi(\theta,\varphi) - \frac{1}{\alpha}[D_\alpha \phi](\theta,\varphi), \quad \alpha \in \mathbb{R}_+^*, \tag{2.7}$$

which obviously satisfies (2.5).

Thus, with the action of rotations and dilations given above, the spherical CWT of a function $f \in L^2(S^2)$, with respect to an admissible wavelet $\psi \in L^2(S^2)$, is defined as

$$W_f(\rho,a) = \langle \psi_{\rho,a} | f \rangle = \int_{S^2} \mathrm{d}\mu(\omega)\, \overline{R_\rho D_a \psi(\omega)}\, f(\omega), \tag{2.8}$$

where $\overline{(\cdot)}$ denotes the complex conjugation. This last expression is nothing but a spherical correlation, i.e.,

$$W_f(\rho,a) = (\psi_a * f)(\rho) \equiv \int_{S^2} \mathrm{d}\mu(\omega)\, \overline{[R_\rho \psi_a]}(\omega) f(\omega). \tag{2.9}$$

The following proposition shows that the family of rotated and translated wavelets constitutes a (continuous) frame in $L^2(S^2)$, from which we derive a reconstruction formula.

[3] The argument in [4,5] applies either to the necessary admissibility conditions (zero mean) or through the asymptotic reasoning corresponding to the Euclidean Limit. For the convenience of the reader, we give in Appendix A a direct proof that the necessary and sufficient admissibility conditions do indeed correspond to each other, which means that any Euclidean wavelet will yield a spherical wavelet.

Proposition 2.1. *Let $f \in L^2(S^2)$. If ψ is an admissible wavelet such that $\int_0^{2\pi} \mathrm{d}\varphi\, \psi(\theta,\varphi) \neq 0$, then*

$$f(\omega) = \int_{\mathbb{R}_+^*} \int_{\mathrm{SO}(3)} \frac{\mathrm{d}a\, \mathrm{d}\nu(\rho)}{a^3} W_f(\rho,a)\big[R_\rho L_\psi^{-1} D_a \psi\big](\omega), \tag{2.10}$$

where $\mathrm{d}\nu(\rho)$ is the left Haar measure on SO(3) *and the coefficients are given by* (2.8). *The* frame operator[4] *L_ψ is defined by*

$$\widehat{[L_\psi h]}(l,m) = G_\psi(l)\hat{h}(l,m), \quad \forall h \in L^2\big(S^2\big), \tag{2.11}$$

where $G_\psi(l)$ is given in (2.4).

The frame so obtained is probably not tight, in general. As a consequence, the spherical CWT does not define an isometry. However, one has the following result, which follows immediately from (2.10):

Corollary 2.2. *Under the conditions of Proposition* 2.1, *the following Plancherel relation is satisfied*:

$$\|f\|^2 = \int_{\mathbb{R}_+^*} \int_{\mathrm{SO}(3)} \frac{\mathrm{d}a\, \mathrm{d}\nu(\rho)}{a^3} \overline{\widetilde{W}_f(\rho,a)} W_f(\rho,a) \tag{2.12}$$

with

$$\widetilde{W}_f(\rho,a) = \big\langle \tilde{\psi}_{\rho,a} \big| f \big\rangle = \big\langle R_\rho L_\psi^{-1} D_a \psi \big| f \big\rangle. \tag{2.13}$$

The proof of these results and more details on the spherical CWT and its implementation can be found in [5] (see also [7] and [17]).

2.2. The axisymmetric case

When working with *axisymmetric* (or zonal) functions, i.e., functions invariant under rotations about the z-axis, the action of rotations is easily understood.

Let us recall that a rotation $\rho \in \mathrm{SO}(3)$ may be parametrized by its Euler angles φ, θ, α ($\varphi, \alpha \in S^1$, $0 \leqslant \theta \leqslant \pi$) in the following way

$$\rho = \rho(\varphi,\theta,\alpha) = r_\varphi^z r_\theta^y r_\alpha^z,$$

where r_γ^u denotes a rotation by an angle γ about the u axis. If g is an axisymmetric function, then $R_\rho g = R_{[\omega]} g$, where $[\omega] = \rho(\varphi,\theta,0)$. In this way, if g is localized around the North Pole η, then $R_{[\omega]} g$ is localized around $\omega = (\theta,\varphi) \in S^2$.

Given $[\omega] = \rho(\varphi,\theta,0) \in SO(3)$, we define the correlation $\star : L^2(S^2) \times L^2(S^2) \to L^2(S^2)$ as

$$(g \star h)(\omega) = \int_{S^2} \mathrm{d}\mu(\omega')\, \overline{R_{[\omega]} g(\omega')} h(\omega'), \tag{2.14}$$

to distinguish it from the complete correlation $*$ given in Eq. (2.9).

Since the stereographic dilation is radial around the North Pole, an axisymmetric wavelet ψ on S^2 remains axisymmetric after dilation. Consequently, the CWT is redefined on $S^2 \times \mathbb{R}_+^*$ by

[4] Also called *resolution operator* in the coherent state literature [3].

$$W_f(\omega, a) = (\psi_a * f)\big([\omega]\big) = (\psi_a \star f)(\omega), \quad a \in \mathbb{R}_+^*. \tag{2.15}$$

In that particular case, the reconstruction formula (2.10) becomes

$$f(\omega) = \int_{\mathbb{R}_+^*} \int_{S^2} \frac{\mathrm{d}a\, \mathrm{d}\mu(\omega')}{a^3} W_f(\omega', a)\big[R_{[\omega]} L_\psi^{-1} D_a \psi\big](\omega'), \tag{2.16}$$

where L_ψ is the frame operator defined in (2.11) with G_ψ reducing to

$$G_\psi(l) = \frac{4\pi}{2l+1} \int_{\mathbb{R}_+^*} \frac{\mathrm{d}a}{a^3} \big|\hat{\psi}_a(l, 0)\big|^2. \tag{2.17}$$

2.3. Practical implementation

In this section, we focus on the implementation aspects of the spherical wavelet transform associated to an axisymmetric wavelet. A more general implementation including directional wavelets may be found in [5] (we may also quote the fast implementation due to McEwen et al. [21]).

Equation (2.15) shows the SCWT as a spherical correlation between functions f and ψ_a. The following proposition shows that the correlation has a simple expression in the Fourier domain.

Proposition 2.3. *Let $f \in L^2(S^2)$ and let $g \in L^2(S^2)$ be axisymmetric. Then*

$$\widehat{(g \star f)}(l, m) = \sqrt{\frac{4\pi}{2l+1}}\, \overline{\hat{g}(l, 0)}\, \hat{f}(l, m), \quad \forall (l, m) \in \mathcal{N}, \tag{2.18}$$

where $\hat{h}$ denotes the Fourier transform of h on S^2 and $\mathcal{N} = \{(l, m)\colon\ l \in \mathbb{N},\ m \in \mathbb{Z},\ |m| \leqslant l\}$.

A proof of this classical result can be found in [12] or [17].

Equations (2.18) and (2.15) suggest a fast implementation of the SCWT in the Fourier domain, which we now detail. We recall that a function $f \in L^2(S^2)$ is *band-limited of bandwidth* $\beta \in \mathbb{N}$ if

$$f \in \mathcal{B}_\beta = \big\{g \in L^2\big(S^2\big)\colon\ \hat{g}(l, m) = 0,\ \forall (l, m) \in \mathcal{N} \text{ such that } l \geqslant \beta\big\}. \tag{2.19}$$

We will work with data discretized on the *equi-angular* grid $\mathcal{G}_B$ defined by

$$\mathcal{G}_B := \big\{(\theta_p, \varphi_q)\colon\ p, q \in \mathbb{Z}[2B]\big\}, \tag{2.20}$$

with $\mathbb{Z}[N] = \{0, \ldots, N-1\}$, $\theta_p = (2p+1)\frac{\pi}{4B}$ and $\varphi_q = q\frac{\pi}{B}$. Actually, $\{\theta_p\}$ constitutes a *pseudo-spectral* grid, localized on the zeros of a Chebyshev polynomial of order 2β [8,12]. The next result, proved in [12], will be of great importance in what follows. It shows that there is a quadrature formula for calculating the Fourier coefficients of band-limited functions.

Proposition 2.4. *Let $g \in \mathcal{B}_\beta$ with $\beta \in \mathbb{N}^0$. Then there exist* weights $w_p^\beta \in \mathbb{R}_+^*$ *such that*

$$\hat{g}(l, m) = \int_{S^2} \mathrm{d}\mu(\theta, \varphi)\, \overline{Y_l^m(\theta, \varphi)} g(\theta, \varphi) \tag{2.21}$$

$$= \sum_{p,q \in \mathbb{Z}[2\beta]} w_p^\beta \overline{Y_l^m(\theta_p, \varphi_q)} g(\theta_p, \varphi_q), \tag{2.22}$$

for all $(l,m) \in \mathcal{N}_\beta = \{(l,m) \in \mathcal{N}\colon\ l < \beta\}$ *and* $(\theta_p, \varphi_q) \in \mathcal{G}_\beta$ *. Explicitly*

$$w_p^\beta = \frac{2\pi}{\beta^2} \sin(\theta_p) \sum_{k \in \mathbb{Z}[\beta]} \frac{1}{2k+1} \sin\bigl((2k+1)\theta_p\bigr), \tag{2.23}$$

with $\sum_{p\in\mathbb{Z}[2\beta]} \sum_{q\in\mathbb{Z}[2\beta]} w_p^\beta = 4\pi$.

Equation (2.22) is in fact a *discrete Fourier transform* on the sphere. The inverse discrete Fourier transform is obtained as

$$g(\theta_p, \varphi_q) = \sum_{(l,m)\in\mathcal{N}_\beta} \hat{g}(l,m) Y_l^m(\theta_p, \varphi_q), \quad p, q \in \mathbb{Z}[2\beta]. \tag{2.24}$$

For l and m fixed, the evaluation of (2.22) needs $O(\beta^2)$ operations. Then for $(l,m) \in \mathcal{N}_\beta$, i.e., β^2 elements, $O(\beta^4)$ operations are needed. The same estimate is valid for the computation of the inverse Fourier transform. The performance of this evaluation may be greatly improved if we note that $Y_l^m(\theta_p, \varphi_q) = n_{lm} P_l^m(\cos\theta_p) e^{im\varphi_q}$, with P_l^m the associated Legendre polynomial of order (l,m) and n_{lm} a normalization constant. Then a discrete Fourier transform on S_1 may be applied on the longitude φ_q in (2.22), which yields

$$\hat{g}(l,m) = \sum_{p,q\in\mathbb{Z}[2\beta]} w_p^\beta g(\theta_p, \varphi_q) \overline{Y_l^m(\theta_p, \varphi_q)} \tag{2.25}$$

$$= \sum_{p\in\mathbb{Z}[2\beta]} w_p^\beta n_{lm} \check{g}(\theta_p, m) P_l^m(\cos\theta_p), \tag{2.26}$$

with $\check{g}(\theta_p, m) = \sum_{q\in\mathbb{Z}[2\beta]} g(\theta_p, \varphi_q) e^{-im\varphi_q}$. The application of a FFT[5] in longitude reduces the complexity to $O(\beta^3 \log\beta)$ operations [5]. Moreover, there exists a fast $O(\beta^2 \log^2\beta)$ algorithm for the spherical Fourier transform developed by Driscoll and Healy [12]. It combines a discrete cosine transform (DCT) over the (co)latitude θ_q and the recurrence rules of Legendre polynomials [33]. A free version[6] of this method, called *SpharmonicKit*, may be found in [24]. These methods are also integrated into the MATLAB© YAWtb toolbox.[7]

2.3.1. The scale range

The range of the scale parameter in the continuous transform seems arbitrary. However, this is not the case in practice. For fixing ideas, let us recall the situation for classical wavelets on $\mathbb{R}$. Even if the wavelet transform of a signal is obtained by integration over the whole real line, in practice, data are discretized and have finite length. Hence the possible values of the scale parameter are constrained on one side by the sampling frequency (this gives a lower bound: the wavelet cannot oscillate more than permitted by the Nyquist frequency) and on the other side by the length of the interval where the signal is defined (upper bound: the wavelet should "live" inside that interval).

In the case of the spherical continuous wavelet transform, the smallest a is also constrained by the sampling frequency of the spherical grid. This phenomenon is displayed on Fig. 2, where $\hat{\psi}_a(l,0)$ is

[5] Fast Fourier transform.

[6] Under GPL license (General Public License [15]).

[7] Developed by some of us and freely (*GPL*ly) available at: http://www.fyma.ucl.ac.be/projects/yawtb.

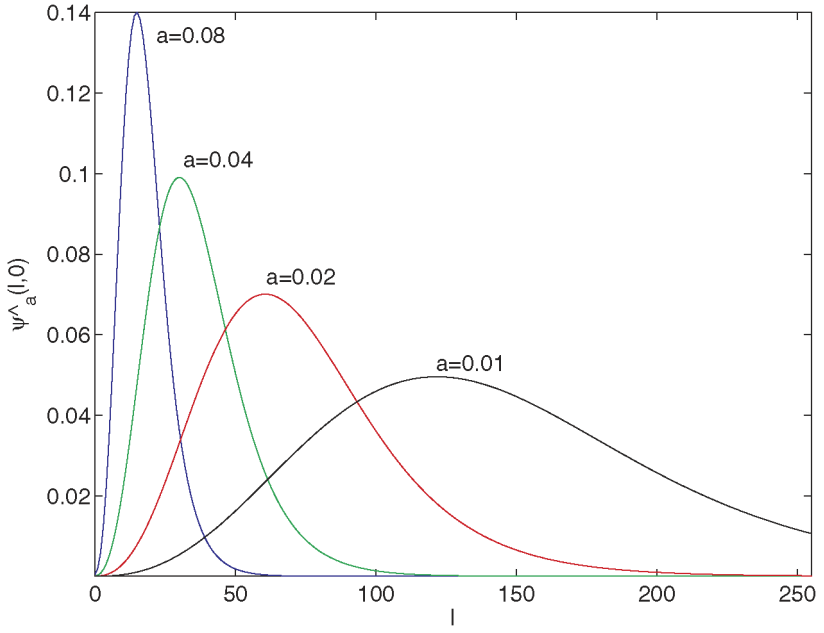

Fig. 2. Behavior of $\hat{\psi}_a(l,0)$ as a function of the scale a. If $a = 0.01$, the bandwidth of the dilated wavelet exceeds the limit fixed by the discretization.

drawn for several values of a. On this graph, we discretize ψ_a on a 512×512 spherical grid according to the previous section, for a maximal permitted bandwidth $\beta = 256$. One clearly sees that $\hat{\psi}(l,0)$ is *not* numerically negligible for $l = 255$ with the choice $a \leqslant 0.01$. Therefore $\psi_a \notin \mathcal{B}_\beta$ and it cannot be defined on $\mathcal{G}_{256}$.

As a matter of fact, the upper limit of the scales is also constrained by the high frequencies of the dilated wavelet. Indeed, the nature of the dilation produces an accumulation of points around the South Pole, so the oscillating tails of the wavelet are compelled to oscillate faster as a increases, even if the amplitude is negligible. The discussion below roughly formalizes this behavior. Before entering it, we emphasize the purely mathematical—and, in fact, irrelevant—aspect of the phenomenon. As we already stressed in [5], going to large values of a is unphysical, wavelet analysis is a *local* tool, whose main function is to detect and characterize (local) discontinuities. Correspondingly, the strong L^p-reconstruction formula, be it with the linear or the bilinear formalism, requires the large scale part of the signal to be treated separately, by projecting it onto a scaling function, instead of a wavelet. Physically, this is to be expected: when scale is important for a given phenomenon, it is the *local* scaling behavior that counts. Good examples are found in statistical mechanics (critical exponents), conformal field theory, or the analysis of fractals.

Now we turn to the mathematical analysis of the large scale behavior of our spherical wavelets. We are going to estimate the highest nonnegligible frequency $l_{\mathrm{M}}(a)$ reached by the dilated wavelet ψ_a, which determines its bandwidth. We will see that it increases not only for small values of the scale (as expected because that corresponds to high frequencies), but also for large ones. Our argument rests upon the fact that the bandwidth of an oscillatory function may be estimated from the distance between its zero crossings.

Given two latitudes α and β in $[0,\pi]$, let us first study the evolution of the (angular) distance between the dilated angles α_a and β_a as a function of a. We get

$$\Delta_{\alpha\beta}(a) := \tan\frac{1}{2}(\alpha_a-\beta_a) = \frac{\tan\frac{1}{2}\alpha_a-\tan\frac{1}{2}\beta_a}{1+\tan\frac{1}{2}\alpha_a\tan\frac{1}{2}\beta_a} = a\left(\frac{\tan\frac{1}{2}\alpha-\tan\frac{1}{2}\beta}{1+a^2\tan\frac{1}{2}\alpha\tan\frac{1}{2}\beta}\right) = \kappa_{\alpha\beta}(a)\Delta_{\alpha\beta}(1)$$

with

$$\kappa_{\alpha\beta}(a) = a\left(\frac{1+\tan\frac{1}{2}\alpha\tan\frac{1}{2}\beta}{1+a^2\tan\frac{1}{2}\alpha\tan\frac{1}{2}\beta}\right). \tag{2.27}$$

If α and β are not zero, the function $\kappa_{\alpha\beta}$ has a unique maximum in

$$\tilde{a}(\alpha,\beta) = \frac{1}{\sqrt{\tan\frac{1}{2}\alpha\tan\frac{1}{2}\beta}}. \tag{2.28}$$

We also have that $\kappa_{\alpha\beta}(0) = \lim_{a\to\infty}\kappa_{\alpha\beta}(a) = 0$. In other words, the distance $\Delta_{\alpha\beta}(a)$ increases in $(0,\tilde{a}]$ and decreases in $[\tilde{a},\infty)$.

Now if the bandwidth of the wavelet is l_0, the minimal distance between two of its zeroes is of the order of $\frac{\pi}{l_0}$. Let us label those points as α and $\beta=\alpha+\frac{\pi}{l_0}$. From the relation $\Delta_{\alpha\beta}(a)=\kappa_{\alpha\beta}(a)\Delta_{\alpha\beta}(1)$, we can see that the bandwidth $l_{\mathrm{M}}(a)$ of the dilated wavelet ψ_a is approximately related to l_0 by

$$\tan\frac{\pi}{2l_{\mathrm{M}}(a)} \simeq \kappa_{\alpha\beta}(a)\tan\frac{\pi}{2l_0},$$

that is to say,

$$l_{\mathrm{M}}(a) \simeq \frac{\pi}{2\tan^{-1}(\kappa_{\alpha\beta}(a)\tan(\frac{\pi}{2l_0}))}. \tag{2.29}$$

Knowing the behavior of $\kappa_{\alpha\beta}(a)$, we can roughly say that $l_{\mathrm{M}}(a)$ decreases in the interval $(0,\tilde{a}]$ and increases in $[\tilde{a},\infty)$ (see Fig. 3).

Taking into account that $\hat{\psi}_a(l,0)$ has noncompact support, another estimate of $l_{\mathrm{M}}(a)$ may be calculated as

$$\check{l}_{\mathrm{M}}(a) = \min\left\{L\in\mathbb{N}\colon\ 0.99\|\psi\|^2 \leqslant \sum_{l=0}^{L}\left|\hat{\psi}_a(l,0)\right|^2 \leqslant \|\psi\|^2\right\}. \tag{2.30}$$

For the particular case of the DOG wavelet, this function is represented in Fig. 3, in solid line, with $a\in[0.025,40]$. We clearly see on this figure, represented in log-log scale, a minimum $l_{\mathrm{M}}=3$ in a neighborhood of $a=0.8$. This means that the DOG wavelet should be discretized on an equi-angular spherical grid of 8×8 points at least and for values of a near 0.8 only. Besides, if we take for example a 256×256 grid ($\beta=128$), the dilated wavelet ψ_a will not be correctly discretized for a outside of the interval $[a_{\mathrm{m}in}=0.0204, a_{\mathrm{M}}=45.83]$ because $l_{\mathrm{M}}(a)$ is strictly bigger than $l=127$ for those values. Notice that, in the *Euclidean approximation* of the stereographic dilation [5], i.e.,

$$D_a\psi(\theta,\varphi) \simeq \frac{1}{a}\psi\left(\frac{1}{a}\theta,\varphi\right), \quad \text{if } a\ll 1, \tag{2.31}$$

the support of $\hat{\psi}_a$ follows the rule

$$\widehat{D_a\psi}(l,0) \simeq \sqrt{a}\hat{\rho}(al), \tag{2.32}$$

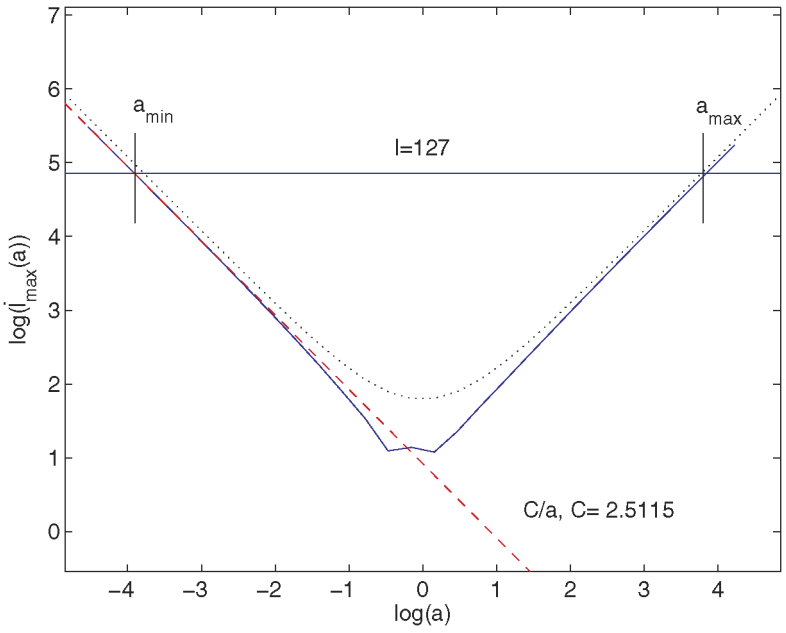

Fig. 3. $\check{l}_{\mathrm{M}}(a)$ as a function of a in solid line (logarithmic representation).

for a particular function $\hat{\rho}:\mathbb{R}_+^* \to \mathbb{R}$ given in [17]. This behavior is confirmed on Fig. 2 where the curves maxima decrease like $\sqrt{a}$. As for wavelets on the line, Eq. (2.32) tells us that the upper bound $l_{\mathrm{M}}(a)$ of the support of $\hat{\psi}_a$ varies like Ca^{-1}, for $C \in \mathbb{R}$. The dashed-line of slope -1 in Fig. 3 shows this evolution in a logarithmic representation of scales. The constant C has been estimated to 2.51 by linear regression on scales $a < 0.04$. The closer the curve $\check{l}_{\mathrm{M}}(a)$ fits this line, the better is the Euclidean approximation. Finally, we plot in dotted-line the approximation (2.29), for a wavelet with bandwidth $l_0 = 6$ and α and β such that $\tan\frac{1}{2}\alpha \tan\frac{1}{2}\beta = 1$. For this value of l_0, this approximation gives a good prediction of $\check{l}_{\mathrm{M}}(a)$ for $a \ll 1$ and $a \gg 1$. However, it does not model correctly the behavior of $\hat{\psi}_a$, in a neighborhood of $a = 1$.

3. Frames revisited

In this section, we describe under which conditions the parameters of the spherical continuous wavelet transform can be discretized without losing the reconstruction property. We start by recalling some basic facts about frames and then introduce a slight generalization of the standard concept, called *controlled* frames.

3.1. Classical frames

Let $\mathfrak{H}$ be a Hilbert space with scalar product $\langle\cdot|\cdot\rangle$ and the associated norm $\|f\| = \sqrt{\langle f|f\rangle}$, $f \in \mathfrak{H}$.

Definition 3.1. Let Γ be a countable set. A family of vectors $\Psi = \{\psi_n \in \mathfrak{H}\colon\ n \in \Gamma\}$ is a discrete frame in $\mathfrak{H}$ if there exist two constants $0 < A \leqslant B < \infty$ such that

$$A\|f\|^2 \leqslant \sum_{n\in\Gamma} \big|\langle \psi_n | f\rangle\big|^2 \leqslant B\|f\|^2, \quad \forall f \in \mathfrak{H}. \tag{3.1}$$

The frame is called *tight* if $A = B$. When $A = B = 1$ and $\|\psi_n\| = 1, \forall n \in \Gamma$, the frame is just an orthonormal basis. Given a frame Ψ, the associated *frame operator* L is defined as

$$Lf = \sum_{n\in\Gamma} \langle \psi_n | f\rangle \psi_n. \tag{3.2}$$

This is, of course, a bounded operator. Indeed [29]:

Proposition 3.2. *If Ψ is a frame of $\mathfrak{H}$, the associated frame operator L is bounded and verifies*

$$A\mathcal{I} \leqslant L \leqslant B\mathcal{I}, \tag{3.3}$$

where $\mathcal{I}$ denotes the unit operator and $P \leqslant Q$ means $\langle g|Pg\rangle \leqslant \langle g|Qg\rangle, \forall g \in \mathfrak{H}$, for two given operators P and Q.

It follows that the frame operator L is not only bounded, it also has a bounded inverse, that is, it belongs to the set $GL(\mathfrak{H})$ [2]. We emphasize that $GL(\mathfrak{H})$ is the natural class of operators in the context of frame theory. Indeed, (3.1) means that the norm $\|\cdot\|$ and the set of coefficients $\{\langle\psi_n|\cdot\rangle\}$ define the same Hilbertian topology on $\mathfrak{H}$. And the elements of $GL(\mathfrak{H})$ are precisely the natural isomorphisms for such a Hilbertian structure, exactly as unitary operators are the isomorphisms for the Hilbert space structure defined by a given inner product $\langle\cdot|\cdot\rangle$ (note the difference between a *Hilbert* space and a *Hilbertian* space: the former is attached to a given inner product, the latter to an equivalence class of inner products).

It is possible to reconstruct a function from its frame coefficients. Let us introduce first a related family of vectors $\tilde{\Psi} = \{\tilde{\psi}_n\colon\ n \in \Gamma\}$ defined by

$$\tilde{\psi}_n = L^{-1}\psi_n. \tag{3.4}$$

Then, we have the following result:

Proposition 3.3. *The family $\tilde{\Psi}$ is a frame with bounds $0 < B^{-1} \leqslant A^{-1} < \infty$, called the* dual frame *of Ψ. Any $f \in \mathfrak{H}$ can be reconstructed from its frame coefficients through*

$$f = \sum_{n\in\Gamma} \langle \psi_n | f\rangle \tilde{\psi}_n = \sum_{n\in\Gamma} \langle \tilde{\psi}_n | f\rangle \psi_n. \tag{3.5}$$

See [11] for a proof. Note that if the frame is tight then $\tilde{\psi}_n = \frac{1}{A}\psi_n$, and the same vectors are used for the decomposition and for the reconstruction. In fact, $\langle Lf|f\rangle = A\|f\|^2$ for every $f \in \mathfrak{H}$, so $L = A\mathcal{I}$ and $L^{-1} = A^{-1}\mathcal{I}$. This is the most attractive property of a tight frame.

Finally, when $A \simeq B$ we can have a good approximation of the element f by setting

$$f \simeq \frac{2}{A+B} Lf = \frac{2}{A+B} \sum_{n\in\Gamma} \langle \psi_n | f\rangle \psi_n, \tag{3.6}$$

since in this case $\frac{2}{A+B} L \simeq \mathcal{I}$.

3.2. Continuous and half-continuous frames

Several variations on the original frame concept have been studied. For instance, it is possible to extend the original definition to the case of continuous decompositions [29], as follows. Let $\mathcal{C}$ be a measurable space with measure $\mathrm{d}\mu(\nu)$. Given a family $\Psi = \{\psi_\nu \in \mathfrak{H}, \nu \in \mathcal{C}\}$, we define the frame operator

$$L : f \in \mathfrak{H} \mapsto Lf = \int_{\mathcal{C}} \mathrm{d}\mu(\nu)\, \langle \psi_\nu | f \rangle \psi_\nu. \tag{3.7}$$

The set Ψ is called a *continuous* frame if L is a bounded operator. This guarantees that $L \in GL(\mathfrak{H})$, and thus also the reconstruction of f from its wavelet coefficients $\{\langle \psi_\nu | f \rangle\}$.

It is also possible to have a mixed set of indices where some of them are continuous while the rest are discrete. If we note by $\nu \in \mathcal{C}$ the continuous set and by $n \in \mathcal{D}$ the discrete one, then we say that the family $\Psi = \{\psi_{\nu,n} \in \mathfrak{H}\colon\ \nu \in \mathcal{C},\ n \in \mathcal{D}\}$ is a frame if there exist two constants $0 < A \leqslant B < \infty$ such that, $\forall f \in \mathfrak{H}$,

$$A\|f\|^2 \leqslant \sum_{n\in\mathcal{D}} \int_{\mathcal{C}} \mathrm{d}\mu(\nu)\, \big|\langle \psi_{\nu,n} | f \rangle\big|^2 \leqslant B\|f\|^2. \tag{3.8}$$

In that case, the family Ψ is called a *half-continuous* frame.

3.3. Controlled and weighted frames

We introduce in this section a slight variation on the definition of frames, called *controlled frames*. It helps tuning the frame bounds in order to obtain a better approximation of f by Lf (as in (3.6)).

3.3.1. Controlled frames

Definition 3.4. Let $O \in GL(\mathfrak{H})$. A frame controlled by the operator O is a family of vectors $\Psi = \{\psi_n \in \mathfrak{H}\colon\ n \in \Gamma\}$ such that there exist two constants $A, B \in \mathbb{R}_+^*$ verifying

$$A\|f\|^2 \leqslant \sum_{n\in\Gamma} \langle \psi_n | f \rangle \langle f | O\psi_n \rangle \leqslant B\|f\|^2, \tag{3.9}$$

for all $f \in \mathfrak{H}$.

In that case, the frame operator is given by

$$L_O f = OLf = \sum_{n\in\Gamma} \langle \psi_n | f \rangle O\psi_n. \tag{3.10}$$

Proposition 3.5. *The family Ψ is a frame of $\mathfrak{H}$ controlled by $O \in GL(\mathfrak{H})$ iff Ψ is a* (*classical*) *frame of* $\mathfrak{H}$.

This result is obtained by projecting $L_O f$ on f and noting that $L_O = OL$. Therefore, if Ψ is controlled by O, there are two constants $A, B \in \mathbb{R}_+^*$ such that

$$A\mathcal{I} \leqslant L_O \leqslant B\mathcal{I} \tag{3.11}$$

$$\Leftrightarrow \quad AO^{-1} \leqslant L \leqslant BO^{-1}, \tag{3.12}$$

with L the classical frame operator defined in (3.2). Since there are two constants $A_O, B_O \in \mathbb{R}_+^*$ such that $A_O \leqslant O \leqslant B_O$, we see that a frame controlled by O with frame bounds $A, B \in \mathbb{R}_+^*$ is a genuine frame with frame bounds AB_O^{-1} and BA_O^{-1}. Conversely, if $A' \leqslant L \leqslant B'$ for $A', B' \in \mathbb{R}_+^*$, then $A'O \leqslant L_O \leqslant B'O$ and $A'A_O \leqslant L_O \leqslant B'B_O$, which proves (3.9).

As a consequence, given a controlled frame Ψ, every function $f \in \mathfrak{H}$ may be reconstructed as in (3.5) without using the operator O. But when $A \simeq B$ in (3.11), $\frac{2}{A+B} L_O$ is close to the identity and we obtain a new approximation for f

$$f \simeq \frac{2}{A+B} L_O f = \frac{2}{A+B} \sum_{n\in\Gamma} \langle \psi_n | f \rangle O\psi_n. \tag{3.13}$$

Thus, if $|B_O/A_O| < |B/A|$, Eq. (3.13) gives a better approximation to f than the one obtained using the frame operator L in (3.6). If, in addition, it turns out that $O\psi_n$ is easily computed, then we have a simple and good reconstruction of f, as desired. Thus, while a controlled frame is equivalent to a classical frame in the mathematical sense, as stated in Proposition 3.5, they can have very different numerical properties.

3.3.2. Weighted frames

A particular case of controlled frame occurs when the operator O is diagonal with respect to the elements ψ_n of the frame Ψ, i.e., if $O\psi_n = w_n\psi_n$ for $w_n \in \mathbb{R}$. Notice that, since O is positive, we have necessarily $w_n > 0$. This diagonalization of the operator O leads to the concept of *weighted* frames.

Definition 3.6. Let $\Psi = \{\psi_n \colon n \in \Gamma \subset \mathbb{Z}\}$ be a family of elements of $\mathfrak{H}$ and $\{w_n \in \mathbb{R}_+^* \colon n \in \Gamma\}$ a sequence of strictly positive weights. We say that this family is a w-frame of $\mathfrak{H}$, if there exist two constants $0 < A \leqslant B < \infty$ such that, for every $f \in \mathfrak{H}$,

$$A\|f\|^2 \leqslant \sum_{n\in\Gamma} w_n \big|\langle \psi_n | f \rangle\big|^2 \leqslant B\|f\|^2. \tag{3.14}$$

In fact, if $w_n > 0$ for all $n \in \Gamma$, a w-frame $\{\psi_n\}$ corresponds to the classical frame $\{\sqrt{w_n}\psi_n\}$. But it will be useful to make these weights more explicit later on. It is interesting to note that the notion of weighted frames was already present in the beginnings of frame theory, as developed by Duffin and Schaeffer [13], in the context of the reconstruction of band-limited signals. They have shown that if $\operatorname{supp}(\hat{f}) \subset [-\frac{\pi}{T}, \frac{\pi}{T}]$, then it is possible to reconstruct the continuous function f from an irregular sampling $\{f(t_n)\}_{n\in\mathbb{Z}}$, by using the frame

$$\left\{ \sqrt{\frac{t_{n+1} - t_{n-1}}{2}} h_T(t - t_n) \colon n \in \mathbb{Z} \right\}, \tag{3.15}$$

where $h_T(t) = \operatorname{sinc}(\frac{\pi t}{T})$. We see that in this case some strictly positive weights $w_n = \sqrt{\frac{t_{n+1}-t_{n-1}}{2}}$ appear, which reflect the particular sampling geometry. We will see in the sequel that similar considerations are needed for an equi-angular spherical sampling.

Even if a weighted frame may also be expressed as a classical frame, we point out that it is possible to define a w-frame operator $L_w : \mathfrak{H} \to \mathfrak{H}$ in this context by

$$L_w f = \sum_{n\in\Gamma} w_n \langle \psi_n | f \rangle \psi_n, \tag{3.16}$$

for every $f \in \mathfrak{H}$. This is an invertible operator [17] and the reconstruction formula for f reads

$$f = L_w^{-1} L_w f = L_w^{-1} \sum_{n\in\Gamma} w_n \langle \psi_n | f \rangle \psi_n = \sum_{n\in\Gamma} w_n \langle \psi_n | f \rangle \tilde{\psi}_n, \tag{3.17}$$

where $\tilde{\psi}_n = L_w^{-1}\psi_n$.

3.3.3. Half-continuous controlled frames

To conclude this section, let us remark that we can define half continuous frames controlled by an operator from $GL(\mathfrak{H})$. In that case, taking the same notations than in Section 3.2, a family $\Psi = \{\psi_{\nu,n} \in \mathfrak{H}\colon\ \nu \in \mathcal{C},\ n \in \mathcal{D}\}$ constitutes such a frame if, for two constants $A, B \in \mathbb{R}_+^*$,

$$A\|f\|^2 \leqslant \sum_{n\in\mathcal{D}} \int_{\nu\in\mathcal{C}} \mathrm{d}\mu(\nu)\, \langle \psi_{\nu,n} | f \rangle \langle f | O\psi_{\nu,n} \rangle \leqslant B\|f\|^2, \tag{3.18}$$

for all $f \in \mathfrak{H}$ and a given $O \in GL(\mathfrak{H})$. As before, it is easy to see that a half-continuous controlled frame is equivalent to a classical half-continuous frame on $\mathfrak{H}$. A particular case arises when O can be factorized in

$$O\psi_{\nu,n} = w_n \tilde{O}\psi_{\nu,n}, \tag{3.19}$$

where $\tilde{O} \in GL(\mathfrak{H})$ and w_n are positive weights. Then, (3.18) becomes

$$A\|f\|^2 \leqslant \sum_{n\in\mathcal{D}} w_n \int_{\nu\in\mathcal{C}} \mathrm{d}\mu(\nu)\, \langle \psi_{\nu,n} | f \rangle \langle f | \tilde{O}\psi_{\nu,n} \rangle \leqslant B\|f\|^2. \tag{3.20}$$

4. Stereographic wavelet frames on the sphere

We come back to the question of the construction of spherical frames starting from the continuous wavelet transform as presented in Section 2. From now on, all wavelets will be assumed to be axisymmetric.

Various alternative constructions of spherical wavelets have been proposed. For example, spherical wavelets based on the lifting scheme were introduced by Schröder and Sweldens [27]. They yield a multiresolution analysis on the sphere based on a particular parametrization of the latter.

Freeden [14] defines also a transformation on S^2 using a special dilation operator defined on the Fourier domain. Polynomial spherical frames have also been introduced in [22] where the order of the polynomials plays the role of the dilation. The drawbacks of these methods is that they focus on the frequential aspect of the transformations. In consequence, the spatial localization of these wavelets is neither guaranteed, nor precisely controlled.

Bülow did succeed in getting good localization properties by using the evolution of a spherical Gaussian governed by the heat equation on S^2 [9]. Then he gets a set of wavelet filters by differentiation of this Gaussian. However, this approach is restricted to the Gaussian function and thus it not as general as the one based on a stereographic dilation applied to an arbitrary admissible wavelet on S^2.

In the following sections, we present two different approaches to the construction of semi-continuous spherical frames. The first one is a straightforward generalization of the classical Euclidean construction. Quite naturally, however, this method does not lead to a tight frame. Indeed, since the continuous version

of the wavelet transform is not an isometry, we cannot expect its discretization to yield a tight frame (discretization usually reduces the quality, i.e., tightness, of frames [6]). We then show that a controlled frame may be constructed in order to get an easy reconstruction of functions from their decomposition coefficients. Finally, a fully discrete frame decomposition is also presented.

4.1. Half-continuous spherical frames

4.1.1. First approach

We propose to discretize the scale of the CWT, but we let the position vary continuously. We choose therefore

$$\omega \in S^2, \quad a \in \alpha = \{a_j \in \mathbb{R}_+^*\colon\ j \in \mathbb{Z},\ a_j > a_{j+1}\}, \tag{4.1}$$

which generates the half-continuous grid

$$\Lambda(\alpha) = \big\{(\omega, a_j)\colon\ \omega \in S^2,\ j \in \mathbb{Z}\big\}. \tag{4.2}$$

To simplify these notations, we will replace in the sequel each occurrence of a_j by j, $\psi_{a_j} = D_{a_j}\psi$ becoming for instance $\psi_j = D_j\psi$, and similarly $W_j(\omega) = \langle \psi_{\omega,j} | f \rangle$.

In order to have a reconstruction of every function $f \in L^2(S^2)$, a first possible approach would be to impose

$$A\|f\|^2 \leqslant \sum_{j\in\mathbb{Z}} \nu_j \int_{S^2} \mathrm{d}\mu(\omega)\, \big|W_j(\omega)\big|^2 \leqslant B\|f\|^2, \tag{4.3}$$

with $A, B \in \mathbb{R}_+^*$ independent of f, and for some weights $\nu_j > 0$ taking into account the discretization of the continuous measure da/a^3. In this case, the family

$$\Psi = \big\{\psi_{\omega,j} = R_{[\omega]} D_j \psi\colon\ \omega \in S^2,\ j \in \mathbb{Z}\big\} \tag{4.4}$$

constitutes a half-continuous frame in $L^2(S^2)$. The following proposition transposes the last condition in the Fourier domain (as identified by spherical harmonics).

Proposition 4.1. *Let ψ be an admissible wavelet. If there are two constants $A, B \in \mathbb{R}_+^*$ such that*

$$A \leqslant \frac{4\pi}{2l+1} \sum_{j\in\mathbb{Z}} \nu_j \big|\hat{\psi}_j(l,0)\big|^2 \leqslant B, \quad \textit{for all } l \in \mathbb{N}, \tag{4.5}$$

then (4.3) *is satisfied.*

Proof. The SCWT of a function $f \in L^2(S^2)$ in the Fourier domain is given by

$$W_f(\omega, a) = \sum_{(l,m)\in\mathcal{N}} \sqrt{\frac{4\pi}{2l+1}}\, \hat{f}(l,m)\overline{\hat{\psi}_a(l,0)} Y_l^m(\omega).$$

Using this expression, we obtain

$$\sum_{j\in\mathbb{Z}} \nu_j \int_{S^2} \mathrm{d}\mu(\omega)\, \big|W_j(\omega)\big|^2 = \sum_{j\in\mathbb{Z}} \nu_j \sum_{(l,k)\in\mathcal{N}} \sum_{(l',k')\in\mathcal{N}} \frac{4\pi}{\sqrt{(2l+1)(2l'+1)}}\, \hat{f}(l,k)\overline{\hat{f}(l',k')}$$

$$\times \overline{\hat{\psi}}_j(l,0)\hat{\psi}_j(l',0)\int_{S^2} \mathrm{d}\mu(\omega)\, Y_l^k(\omega)\overline{Y_{l'}^{k'}(\omega)}$$

$$= \sum_{j\in\mathbb{Z}} \nu_j \sum_{(l,k)\in\mathcal{N}} \frac{4\pi}{2l+1}\left|\hat{f}(l,k)\right|^2\left|\hat{\psi}_j(l,0)\right|^2$$

$$= \sum_{(l,k)\in\mathcal{N}} \left|\hat{f}(l,k)\right|^2 \sum_{j\in\mathbb{Z}} \frac{4\pi}{2l+1}\nu_j\left|\hat{\psi}_j(l,0)\right|^2,$$

where we have used the orthonormality of the spherical harmonics. The lower and upper bounds in (4.3) are well defined if there are two constants $A, B \in \mathbb{R}_+^*$ such that

$$A \leqslant \frac{4\pi}{2l+1}\sum_{j\in\mathbb{Z}} \nu_j\left|\hat{\psi}_j(l,0)\right|^2 \leqslant B, \quad \text{for all } l \in \mathbb{N}. \qquad \square$$

In order to illustrate this result, let us choose a DOG wavelet ($\alpha = 1.25$) and a discretized dyadic scale with a certain number of voices $K \in \mathbb{N}^0$ per octave, namely,

$$a_j = a_0 2^{-j/K}, \quad j \in \mathbb{Z}. \tag{4.6}$$

For the sake of simplicity, we replace the indices a_j by j. Moreover we choose weights ν_j that take into account the discretization of the continuous measure da/a^3, which means

$$\nu_j = \frac{a_j - a_{j+1}}{a_j^3} = \frac{2^{1/K}-1}{2^{1/K}a_j^2}. \tag{4.7}$$

We have estimated the bounds A and B, respectively, by the minimum and the maximum of the quantity

$$S(l) = \frac{4\pi}{2l+1}\sum_{j\in\mathbb{Z}} \nu_j\left|\hat{\psi}_j(l,0)\right|^2, \tag{4.8}$$

over $l \in [0, 31]$ and for $K = 1, 2, 3, 4$. The function $S(l)$ is represented on Fig. 4 for $K \leqslant 3$ and the results are shown in Table 1. We see that for $K > 2$, the ratio B/A converges toward the value 1.8107. We thus do not obtain a tight frame, for which we should have $A = B$. As can be checked on the graph, however, $S(l)$ quickly tends to a constant for $l \geqslant 5$. The problem mostly comes from a severe "dip" in the graph of $S(l)$ (Fig. 4) for small values of l ($l \leqslant 3$).

4.1.2. Second approach

Trying to converge to a tight frame, we adopt now a second approach for our half-continuous discretization. We start from the Plancherel relation defined in Corollary 2.2 and determine under which conditions we can obtain a *controlled* frame. That is, for two frame bounds $A, B \in \mathbb{R}_+^*$, we want

$$A\|f\|^2 \leqslant \sum_{j\in\mathbb{Z}} \nu_j \int_{S^2} \mathrm{d}\mu(\omega)\, W_j(\omega)\overline{\widetilde{W}}_j(\omega) \leqslant B\|f\|^2, \tag{4.9}$$

where $f \in L^2(S^2)$ and $\widetilde{W}_j(\omega) = \langle R_{[\omega]}L_\psi^{-1}D_j\psi|f\rangle$. The operator L_ψ^{-1} controlling the frame is the continuous frame operator defined in the Fourier domain by

$$\widehat{L_\psi^{-1}f}(l,m) = G_\psi^{-1}(l)\,\hat{f}(l,m),$$

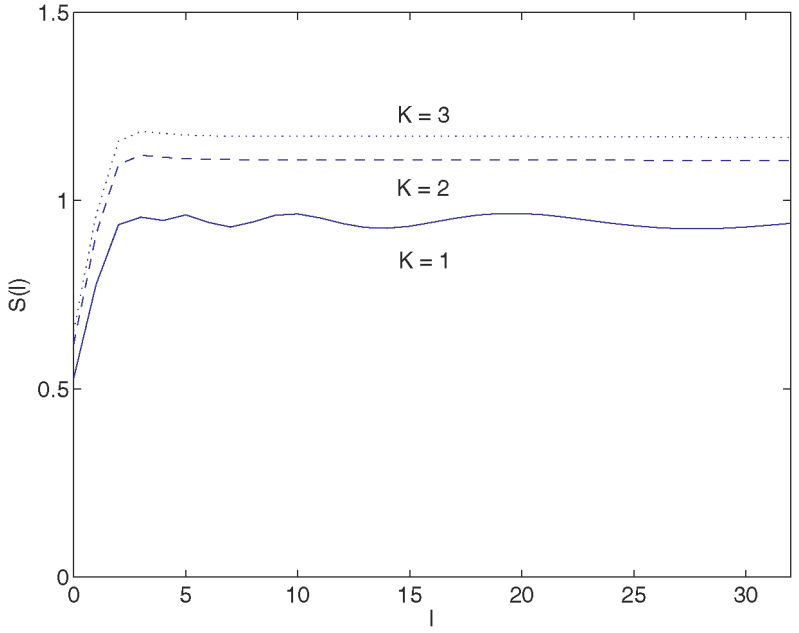

Fig. 4. The function $S(l)$ for $l \in [0, 31)$ and $K = 1, 2, 3$. First approach.

Table 1
Estimation of the bounds A and B as a function of the extrema of $S(l)$ for some values of K. First approach

K	A	B	B/A
1	0.5281	0.9658	1.8288
2	0.6817	1.1203	1.8107
3	0.6537	1.1836	1.8107
4	0.6722	1.2171	1.8107

where G_ψ is given in (2.17). It is bounded with bounded inverse, i.e., $L_\psi \in GL(\mathcal{H})$, if and only if the wavelet ψ is admissible.

Proposition 4.2. *If there exist two constants* $A, B \in \mathbb{R}_+^*$ *such that*

$$A \leqslant \frac{4\pi}{2l+1} G_\psi(l)^{-1} \sum_{j\in\mathbb{Z}} \nu_j \left|\hat{\psi}_j(l,0)\right|^2 \leqslant B, \quad \text{for all } l \in \mathbb{N}, \tag{4.10}$$

then (4.9) *is satisfied.*

Proof. As in the previous proposition, we start from the Fourier coefficients

$$W_f(\omega, a) = \sum_{(l,m)\in\mathcal{N}} \sqrt{\frac{4\pi}{2l+1}}\, \hat{f}(l,m)\overline{\hat{\psi}_a(l,0)} Y_l^m(\omega).$$

Then $\widetilde{W}_f(\omega,a)=\langle R_{[\omega]}L_\psi^{-1}D_a\psi\,|\,f\rangle$ reads

$$\widetilde{W}_f(\omega,a)=\sum_{(l,m)\in\mathcal{N}}\sqrt{\frac{4\pi}{2l+1}}G_\psi(l)^{-1}\hat{f}(l,m)\overline{\hat{\psi}_a(l,0)}Y_l^m(\omega),$$

since the frame operator depends only on l and commutes with rotations.

Using these expressions for the coefficients and the fact that spherical harmonics are orthonormal, we find

$$\sum_{j\in\mathbb{Z}}\nu_j\int_{S^2}\mathrm{d}\mu(\omega)\,W_j(\omega)\overline{\widetilde{W}_j(\omega)}=\sum_{(l,k)\in\mathcal{N}}\big|\hat{f}(l,k)\big|^2\sum_{j\in\mathbb{Z}}\frac{4\pi}{2l+1}G_\psi(l)^{-1}\nu_j\big|\hat{\psi}_j(l,0)\big|^2.$$

Then, inequalities in (4.9) are verified if there exist two constants A, $B\in\mathbb{R}_+^*$, such that

$$A\leqslant\frac{4\pi}{2l+1}G_\psi(l)^{-1}\sum_{j\in\mathbb{Z}}\nu_j\big|\hat{\psi}_j(l,0)\big|^2\leqslant B,\quad\text{for all } l\in\mathbb{N}.\qquad\square$$

Note that, for $a_j=a_0 2^{-j/K}$,

$$G_\psi(l)=\lim_{K\to\infty}\frac{4\pi}{2l+1}\sum_{j\in\mathbb{Z}}\nu_j\big|\hat{\psi}_j(l,0)\big|^2,\tag{4.11}$$

since the weights ν_j discretize the continuous measure $\mathrm{d}a/a^3$ (in other words, G_ψ is well approximated by Riemann sums). Therefore, we obtain a good approximation of G_ψ by taking a large K in the previous equation. We will set $K=10$.

Given this scale discretization and using the same wavelet and the same weights ν_j as in the first approach, the new quantity

$$S(l)=\frac{4\pi}{2l+1}G_\psi(l)^{-1}\sum_{j\in\mathbb{Z}}\nu_j\big|\hat{\psi}_j(l,0)\big|^2\tag{4.12}$$

has been evaluated. It is drawn on Fig. 5 for several values of K. The previous "dip" at small l has disappeared and the oscillations occurring at $K=1$ are almost inexistent for $K=3$. This is confirmed in Table 2, where the values of A and B have been estimated by the infimum and the supremum of $S(l)$ on $l\in[0,31]$, respectively. We see that the ratio B/A tends quickly to 1 as K increases. A tight frame is thus reachable using the controlled frame approach.

4.1.3. Reconstruction

A function $f\in L^2(S^2)$ can be reconstructed from its coefficients $W_j(\omega)$ as soon as the family $\Psi=\{\psi_{\omega,j}\colon\ \omega\in S^2,\ j\in\mathbb{Z}\}$ constitutes a (classical) half-continuous frame.

Proposition 4.3. *Let $\alpha=\{a_j\colon\ j\in\mathbb{Z},\ a_j>a_{j+1}\}$ be a sequence of scales. If ψ is an axisymmetric wavelet such that, for two constants A, $B\in\mathbb{R}_+^*$,*

$$A\leqslant g_\psi(l)=\frac{4\pi}{2l+1}\sum_{j\in\mathbb{Z}}\nu_j\big|\hat{\psi}_j(l,0)\big|^2\leqslant B,\quad\forall l\in\mathbb{N},\tag{4.13}$$

then,

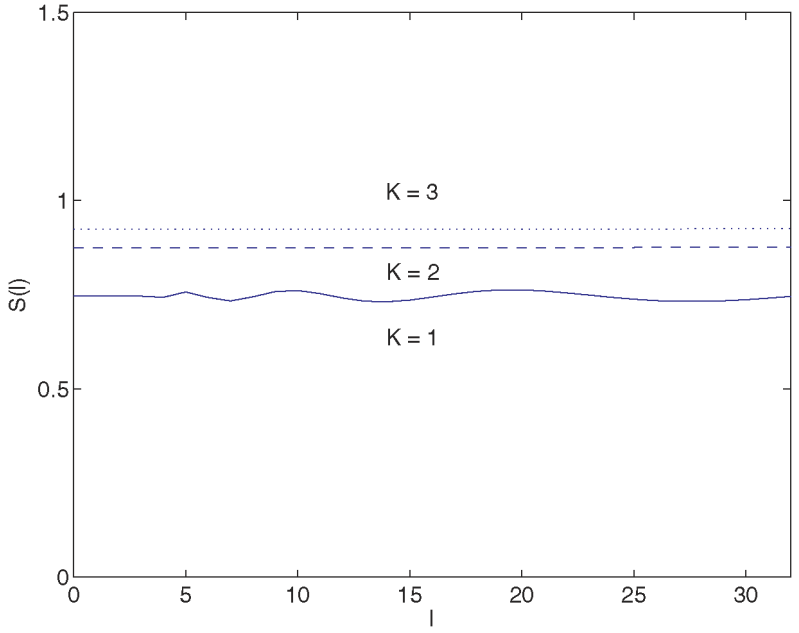

Fig. 5. The function $S(l)$ for $l \in [0, 31[$ and $K = 1, 2, 3$. Second approach.

Table 2
Estimation of the bounds A and B as a function of the extrema of $S(l)$ for some values of K. Second approach

K	A	B	B/A
1	0.7313	0.7628	1.0431
2	0.8747	0.8766	1.0021
3	0.9242	0.9254	1.0014
4	0.9503	0.9512	1.0009

$$f(\omega) = \sum_{j\in\mathbb{Z}} \nu_j \int_{S^2} \mathrm{d}\mu(\omega') \left[R_{[\omega]} \ell_\psi^{-1} D_{a_j} \psi\right](\omega') W_f(\omega', a_j) = \sum_{j\in\mathbb{Z}} \nu_j [\underline{\psi}_j \star W_j](\omega),$$

where ℓ_ψ is the operator defined in the Fourier domain by

$$\widehat{[\ell_\psi^{-1} h]}(l, m) = g_\psi^{-1}(l) h(l, m). \tag{4.14}$$

and $\underline{\psi}_j = \ell_\psi^{-1} \psi_j$ is the dual function of ψ_j.

The proof is similar to the proof of Proposition 4.2, replacing G_ψ by g_ψ. The new operator ℓ_ψ is nothing but the discretization of L_ψ defined in (2.17). According to this proposition, the family Ψ can be interpreted as a tight frame controlled by the operator ℓ_ψ^{-1}.

We have seen in Section 2.3.1 that there exists a limit scale $\tilde{a} \in \mathbb{R}_+^*$ such that, for increasing $a \in [\tilde{a}, \infty[$, the support of $\tilde{\psi}_a$ stops contracting toward low frequencies and starts growing again toward high

frequencies. We will lump together all wavelets having this behavior into a single scaling function ζ defined by

$$\left|\hat{\zeta}(l,m)\right|^2 = \delta_{m,0} \sum_{j=-\infty}^{-1} \nu_j \left|\hat{\psi}_j(l,0)\right|^2. \tag{4.15}$$

On the example depicted in Fig. 3, $\tilde{a} \simeq 0.8$. Thus we can safely take $\tilde{a} = 1$, corresponding to $j = 0$. This justifies the upper bound in the sum (4.15). However, the weights $\nu_j \propto a_j^{-2}$ decrease rapidly for $j \to -\infty$ (large scales), so that only the last few terms, with $|j]$ small, will contribute significantly to the sum, which entails that the function ζ is mainly concentrated at low frequencies. This behavior can be seen again on Fig. 3 and can also be checked numerically.

In addition, if the analyzed signal f is band-limited, i.e., there is a bandwidth $\beta \in \mathbb{N}^0$ such that $f \in \mathcal{B}_\beta$ (a frequent situation for signals on the sphere), we may define a *residual* function with

$$\left|\hat{\eta}(l,m)\right|^2 = \mathbb{1}_{[0,\beta)}(l)\delta_{m,0} \sum_{j=J+1}^{\infty} \nu_j \left|\hat{\psi}_j(l,0)\right|^2, \tag{4.16}$$

where J is the maximal resolution such that the support of $\hat{\psi}_j(l,0)$ is contained in $[0,\beta)$.

This function will catch the high frequency components of f omitted by $\hat{\psi}_j$ for $j \in [0,J]$. With these two functions, the reconstruction formula reads

$$f(\omega) = [\,\underline{\bar{\zeta}} \star S](\omega) + \sum_{j=0}^{J} \nu_j [\,\underline{\bar{\psi}}_j \star W_j](\omega) + [\,\underline{\bar{\eta}} \star H](\omega), \tag{4.17}$$

with $S(\omega) = \langle R_{[\omega]}\zeta \,|\, f\rangle$, $\underline{\zeta} = \ell_\psi^{-1}\zeta$, $H(\omega) = \langle R_{[\omega]}\eta \,|\, f\rangle$, and $\underline{\eta} = \ell_\psi^{-1}\eta$.

4.2. Discrete spherical frames

As a last step, we will now completely discretize the CWT on the sphere. First, the scales are discretized as previously, namely

$$a \in \alpha := \{a_j \in \mathbb{R}_+^* \colon\ a_j > a_{j+1},\ j \in \mathbb{Z}\}.$$

Then we choose the positions on an equi-angular grid of resolution j and of size $2\beta_j \times 2\beta_j$ ($\beta_j \in \mathbb{N}$), i.e.,

$$\omega \in \mathcal{G}_j := \left\{ \omega_{jpq} = (\theta_{jp}, \varphi_{jq}) \in S^2 \colon\ \theta_{jp} = \frac{(2p+1)\pi}{4\beta_j},\ \varphi_{jq} = \frac{q\pi}{\beta_j},\ p,q \in \mathbb{Z}[2\beta_j] \right\}. \tag{4.18}$$

As explained in Section 2.3, the grid $\mathcal{G}_j$ allows to sample perfectly any function of bandwidth β_j.

The complete grid finally reads as follows:

$$\Lambda(\alpha,\beta) = \left\{(a_j, \omega_{jpq}) \colon\ j \in \mathbb{Z},\ p,q \in \mathbb{Z}[2\beta_j]\right\}, \tag{4.19}$$

for a set of bandwidths $\beta = \{\beta_j \in \mathbb{N} \colon\ j \in \mathbb{Z}\}$. In this case, for an axisymmetric admissible mother wavelet $\psi \in S^2$, the family

$$\Psi = \left\{\psi_{jpq} = R_{[\omega_{jpq}]} D_j \psi \colon\ j \in \mathbb{Z},\ p,q \in \mathbb{Z}[2\beta_j]\right\} \tag{4.20}$$

constitutes a weighted frame controlled by the operator L_ψ^{-1}, if there are two constants $A, B \in \mathbb{R}_+^*$ such that, for any $f \in L^2(S^2)$,

$$A\|f\|^2 \leqslant \sum_{j\in\mathbb{Z}} \sum_{p,q\in\mathbb{Z}[2\beta_j]} \nu_j w_{jp} W_j[p,q]\overline{\widetilde{W}_j[p,q]} \leqslant B\|f\|^2, \tag{4.21}$$

with $W_j[p,q] = \langle \psi_{jpq} | f\rangle$, $\widetilde{W}_j[p,q] = \langle L_\psi^{-1}\psi_{jpq}|f\rangle$, and where the quadrature weights $w_{jp} = w_p^{\beta_j}$ are defined in (2.23). The product $\nu_j w_{jp}$ replaces the continuous measure $a^{-3}\,\mathrm{d}a\,\mathrm{d}\mu(\theta,\varphi)$ of the continuous framework.

Proposition 4.4. *Consider the discretization grid $\Lambda(\alpha,\beta)$ defined in* (4.19)*. Given an axisymmetric admissible wavelet ψ on S^2, define the quantities*

$$S'(l) = \sum_{j\in\mathbb{Z}} \frac{4\pi\nu_j}{2l+1} \mathbb{1}_{[0,\beta_j)}(l) G_\psi^{-1}(l) \big|\hat{\psi}_j(l,0)\big|^2, \tag{4.22}$$

$$\delta = \|\mathcal{X}\| \equiv \sup_{(H_l)_{l\in\mathbb{N}}} \frac{\|\mathcal{X}H\|}{\|H\|}, \tag{4.23}$$

where the infinite matrix $(\mathcal{X}_{ll'})_{l,l'\in\mathbb{N}}$ is given by

$$\mathcal{X}_{ll'} = \sum_{j\in\mathbb{N}} \frac{2\pi\nu_j c_j(l,l')}{\beta_j} \mathbb{1}_{[2\beta_j,\infty)}(l+l') G_\psi^{-1}(l) \big|\hat{\psi}_j(l,0)\big| \big|\hat{\psi}_j(l',0)\big| \tag{4.24}$$

and $c_j(l,l') = (2(l+\beta_j)+1)^{1/2}(2(l'+\beta_j)+1)^{1/2}$. If we have

$$0 \leqslant \delta < K_0 \leqslant K_1 < \infty, \tag{4.25}$$

where $K_0 = \inf_{l\in\mathbb{N}} S'(l)$ and $K_1 = \sup_{l\in\mathbb{N}} S'(l)$, then the family (4.20) *is a weighted spherical frame controlled by the operator L_ψ^{-1}, with frames bounds $K_0 - \delta$, $K_0 + \delta$.*

The proof of this proposition is quite technical and may be found in Appendix B.

The evaluation of $\|\mathcal{X}\|$ could be complex when the size of $\mathcal{X}$ is infinite. In practice, however, we work with band-limited functions $f \in L^2(S^2)$ of bandwidth $\beta_M \in \mathbb{N}^0$. In this case $\|\mathcal{X}\|$ can be replaced by the norm of the finite matrix $(\mathcal{X}_{l,l'})_{0\leqslant l,l'<\beta_M}$.

We have estimated the bounds of a spherical DOG wavelet frame in the case $\beta_M = 128$, using a dyadically discretized scale (with $K = a_0 = 1$ in (4.6)), while the bandwidth associated to the grid size supporting each resolution j was fixed to

$$\beta_j = \beta_0 2^{|j|}, \quad \beta_0 \in \mathbb{N}, \tag{4.26}$$

where β_0 is the minimal bandwidth associated to ψ_1. The last equation takes into account the particular nature of the stereographic dilation on S^2. Indeed, for the DOG wavelet, Fig. 3 shows that the (numerical) support of $\hat{\psi}_j$ increases roughly with $2^{|j|}$.

Table 3 presents the results of the evaluation of K_0, K_1, and δ as well as the bounds of the associated frames. One can see that condition (4.25) is satisfied for $\beta_0 \geqslant 4$. However, a tight frame cannot be obtained by increasing β_0. Indeed if β_0 tends to infinity, the spherical grids at each resolution become finer and finer and we approach half-continuous frames. But, as seen in the previous section, this single voice discretization of the scale is not sufficient for producing a tight frame.

Table 3
Evaluation of K_0, K_1, and δ on the functions $f \in L^2(S^2)$ at bandwidth 128

	K_0	K_1	δ	$A = K_0 - \delta$	$B = K_1 + \delta$	B/A
$\beta_0 = 2$	0.6691	0.7644	344.2417	–	–	–
$\beta_0 = 4$	0.7313	0.7736	0.0607	0.6707	0.8343	1.2440
$\beta_0 = 8$	0.7313	0.7736	0.0014	0.7299	0.7751	1.0618

4.2.1. Approximate reconstruction

As explained in Section 3.3.1, the frame $\Psi = \{\psi_{jpq}\}$ controlled by L_ψ^{-1} provides a simple approximate reconstruction formula if the bounds A and B are sufficiently close. In this case, indeed, we have

$$f(\omega) \simeq \frac{2}{A+B} \sum_{j\in\mathbb{Z}} \sum_{p,q\in\mathbb{Z}[2\beta_j]} \nu_j w_{jp} W_j[p,q]\big[L_\psi^{-1}\psi_{jpq}\big](\omega). \tag{4.27}$$

Let us assume that f is a band-limited function, i.e., $f \in \mathcal{B}_{\beta_M}$, for a certain $\beta_M \in \mathbb{N}$. Therefore, f may be discretized without loss of information on a grid $\mathcal{G}_J$, where $J \in \mathbb{N}^0$ is the maximal resolution of the grid such that $\beta_J = \beta_M$. As in the half-continuous case, the residual function η defined in (4.16) can be used to catch the high frequencies left over by the restriction $j \leqslant J$.

This leads to the approximate reconstruction formula

$$\begin{aligned}\frac{A+B}{2} f(\omega) \simeq{}& \sum_{j=-J}^{J} \sum_{p,q\in\mathbb{Z}[2\beta_j]} \nu_j w_{jp} W_j[p,q]\big[L_\psi^{-1}\psi_{jpq}\big](\omega) \\ &+ \cdots + \sum_{p,q\in\mathbb{Z}[2\beta_M]} H[p,q]\big[L_\psi^{-1}\eta_{pq}\big](\omega),\end{aligned} \tag{4.28}$$

where $H[p,q] = \langle \eta_{pq} | f \rangle$ and $\eta_{pq}(\omega) = [R_{[\omega_{Jpq}]}\eta](\omega)$.

Notice that a scaling function could be defined to gather wavelets in the range $j < -J$. However, wavelet coefficients at these resolutions are practically negligible since the weights ν_j decrease with j as 2^{2j}. The approximation of f by the new frame operator

$$\begin{aligned}L'_\psi f = {}& \frac{2}{A+B} \sum_{j=-J}^{J} \sum_{p,q\in\mathbb{Z}[2\beta_j]} \nu_j w_{jp} W_j[p,q] L_\psi^{-1}\psi_{jpq} \\ &+ \cdots + \frac{2}{A+B} \sum_{p,q\in\mathbb{Z}[2\beta_M]} H[p,q] L_\psi^{-1}\eta_{pq},\end{aligned} \tag{4.29}$$

may be largely improved by using the *conjugate gradient algorithm* [19], which computes iteratively, from L'_ψ, the reconstruction of f that we would obtain with the dual wavelets of ψ_n. Note the latter cannot be obtained explicitly, because we cannot control the effect in Fourier space of the undersampling implied by the successive grids.

4.2.2. An example

To conclude, we will now decompose and reconstruct a particular example of spherical data, namely, the global average elevation map of the Earth. The original data f (Fig. 6(a)) represent elevations relatively to the mean level of the oceans (in meters) and are recorded on an equi-angular grid of 512×512

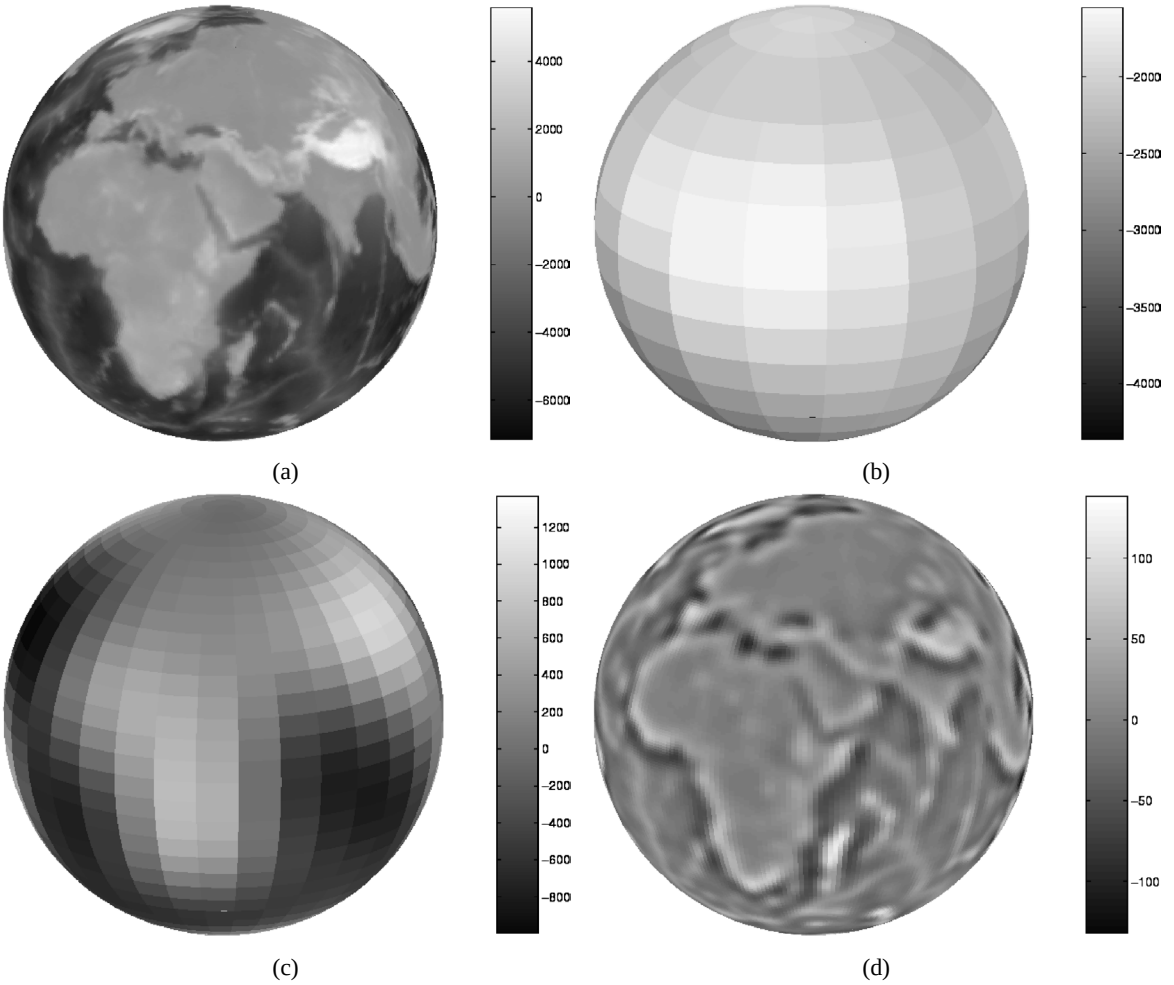

Fig. 6. Decomposition of the Earth elevation map. (a) Global average elevation data (512 × 512 equi-angular grid). The elevations are relative to the mean level of the oceans (in meter). (b) $W_0[p,q]$. (c) $W_3[p,q]$. (d) $W_6[p,q]$.

points ($\beta_{\mathrm{M}} = 256$). Notice this is a purely illustrative example and is not meant to provide a technique for modeling real geophysical data.

The mother wavelet used for the frame decomposition is the DOG ($\alpha = 1.25$). The parameters of the multi-scale grid $\Lambda(\alpha, \beta)$ are $a_0 = 1$ and $\beta_0 = 4$, for scales and bandwidths discretized as in (4.6) (with $K = 1$) and (4.26). According to the original spherical grid ($\beta_{\mathrm{M}} = 256$), the maximum resolution is thus $J = 6$. The values $W_j[p,q]$ have been obtained by computing $W_f(\omega, a_j)$ on the maximum grid $\mathcal{G}_J$, and by estimating then the coefficients $W_f(\omega_{jpq}, a_j)$ by bilinear interpolation of the coefficients $W_f(\omega_{Jp'q'}, a_j)$ on the sub-grid $\mathcal{G}_j$. We use this method because this grid is *not* included into the maximum one, i.e., $\mathcal{G}_j \nsubseteq \mathcal{G}_J$ for all $|j| < J$. Figures 6(b), 6(c), and 6(d) show respectively wavelet coefficients $W_0[p,q]$, $W_3[p,q]$, and $W_6[p,q]$. We clearly see the multiscale decomposition of f on grids adapted to data resolution. We may remark also that the Himalaya mountains behave like a singularity across scales.

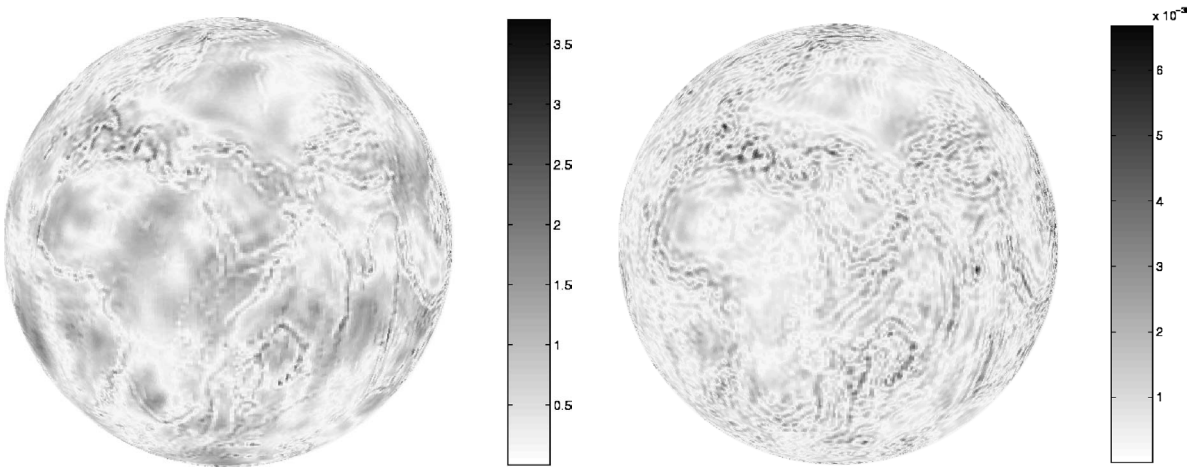

(a) (b)

Fig. 7. (a) Difference between the elevation map f and its approximation Lf. (b) Difference between f and its reconstruction $f^{(3)}$ obtained after three iterations of the conjugate gradient algorithm. For (a) and (b), the values are in percentage of the maximum value of the original data.

For the approximate reconstruction of the elevation map, the function $G_\psi(l)$ used in the definition of the operator L_ψ has been first estimated with the help of (4.11) taking $K = 10$ voices. In addition, the ratio $\frac{2}{A+B}$ occurring in (4.27) has been set to 1.3289 from the results shown in Table 3. The difference $f - L'_\psi f$ between original data and the reconstruction is given on Fig. 7(a). As shown by the amplitudes of this difference (given in percentage of the maximum of f), the reconstruction $L'_\psi f$ is very close to f.

A better reconstruction yet is obtained with the conjugate gradient algorithm. Figure 7(b) displays the difference between f and the approximation $f^{(3)}$ computed after only 3 steps. The amplitudes of $f - f^{(3)}$ are tiny in comparison with those of $f - L'_\psi f$ (about 600 times smaller). This effect appears also in the relative errors:

$$\frac{\|f - L'_\psi f\|}{\|f\|} \simeq 1.1\%, \tag{4.30}$$

$$\frac{\|f - f^{(3)}\|}{\|f\|} \simeq 2 \times 10^{-3}\%. \tag{4.31}$$

5. Outcome

In this paper, we have designed frames of spherical wavelets. Our construction has two distinguished features. First, it is based on the *spherical continuous wavelet transform* introduced in [4,5]. Thus we use genuine spherical wavelets, whose multiscale localization is precisely controlled. Second, our sampling scheme makes use of the very simple equi-angular grids, which are widespread in spherical data processing.

We have introduced two variants of spherical frames. The first one, the quasi-continuous frames, features a continuous translation variable and discrete scales, very much in the idea of the dyadic wavelet transform. The second one yields fully discrete frames, where all parameters are sampled. A careful

analysis of these constructions led us to introduce the idea of controlled frames, which reflect in this case the particular nature of the spherical theory. Working with equi-angular grids allowed us to introduce fast algorithms based on the fast spherical Fourier transform. Finally we have tested these frames on a set of natural data, using successively two particular reconstruction procedures.

Spherical wavelet frames offer a very flexible tool whenever data are inherently bound to spherical geometry. This is particularly the case in astronomy and astrophysics, where spherical wavelets have become one of the main tools for analyzing the Cosmic Microwave Background (see [10] or [34] for a recent survey and further references). But it is also true in fields such as geophysics and remote sensing, for example. Spherical wavelet frames offer a way to model efficiently functions that are deformations of a spherical base and could thus be of interest in computer graphics [9,23] and in computational chemistry, where one wants to represent and study electrical potential surfaces [20]. A similar situation occurs with certain problems in acoustics [18]. In computational vision, spherical frames seem a strong candidate for an efficient study of the plenoptic function. They also share a strong common geometric base with conformal (projective) vision [1,31,32]. Finally, with the development of image based rendering and omnidirectional cameras, spherical wavelets clearly provide a natural way toward processing these new sources of data. More specifically, they allow one to extend efficient multiresolution algorithms to the omnidirectional case. A concrete example is given in [30], where spherical wavelets are used for multiresolution motion compensation. Another obvious application would be in compression of omnidirectional images.

Acknowledgments

We thank the anonymous referees for some constructive remarks that have improved the clarity of the paper. I.B. and P.V. acknowledge the support of the Swiss National Science Foundation through Grant FNS 200021-101880/1. M.M. was supported by the European Union mobility program RTN2-2001-00507.

Appendix A. Stereographic construction of spherical wavelets

In this appendix, we prove explicitly that full admissibility of Euclidean wavelets yields full admissibility of spherical wavelets [this proof originates from a discussion with M. Fornasier and H. Rauhut; we thank them both].

Proposition A.1. *Any admissible wavelet on $L^2(\mathbb{R}^2)$ yields an admissible wavelet on $L^2(S^2)$ by inverse stereographic projection.*

Proof. As stated in [4], the stereographic projection (see Fig. 1) is the map $\Xi : L^2(S^2, \mathrm{d}\mu) \to L^2(\mathbb{R}^2, r\,\mathrm{d}r\,\mathrm{d}\varphi)$ given by

$$\Xi : f(\theta, \varphi) \mapsto \frac{2}{1+r^2} f(2\arctan r, \varphi). \tag{A.1}$$

The map Ξ is unitary and satisfies the intertwining relation

$$\Xi D_a = D_a^p \Xi, \tag{A.2}$$

where D_a is the stereographic dilation (2.2) on S^2 and D_a^p is the usual unitary plane dilation, defined as

$$D_a^p f(r,\varphi) = a^{-1} f\left(a^{-1}r, \varphi\right). \tag{A.3}$$

The admissibility of a wavelet $\psi \in L^2(S^2)$ can be written as

$$I = \int_{\mathrm{SO}(3)} \mathrm{d}\nu(\rho) \int_0^\infty \frac{\mathrm{d}a}{a^3} \left|\langle R_\rho D_a \psi | \phi \rangle\right|^2 < \infty, \quad \forall \phi \in L^2\left(S^2\right), \tag{A.4}$$

where $\mathrm{d}\nu$ is the invariant (Haar) measure on SO(3) and R_ρ is the rotation matrix associated to $\rho \in \mathrm{SO}(3)$.

Introducing the unitary map Ξ, we get

$$\begin{aligned} I &= \int_{\mathrm{SO}(3)} \mathrm{d}\nu(\rho) \int_0^\infty \frac{\mathrm{d}a}{a^3} \left|\left\langle D_a \psi \middle| R_\rho^{-1}\phi\right\rangle_{L^2(S^2)}\right|^2 = \int_{\mathrm{SO}(3)} \mathrm{d}\nu(\rho) \int_0^\infty \frac{\mathrm{d}a}{a^3} \left|\left\langle \Xi D_a \psi \middle| \Xi R_\rho^{-1}\phi\right\rangle_{L^2(\mathbb{R}^2)}\right|^2 \\ &= \int_{\mathrm{SO}(3)} \mathrm{d}\nu(\rho) \int_0^\infty \frac{\mathrm{d}a}{a^3} \left|\left\langle D_a^p \Xi \psi \middle| \Xi R_\rho^{-1}\phi\right\rangle_{L^2(\mathbb{R}^2)}\right|^2. \end{aligned}$$

Defining $\psi^p \equiv \Xi\psi$, we obtain finally

$$I = \int_{\mathrm{SO}(3)} \mathrm{d}\nu(\rho) \int_0^\infty \frac{\mathrm{d}a}{a^3} \left|\left\langle D_a^p \psi^p \middle| \Xi R_\rho^{-1}\phi\right\rangle_{L^2(\mathbb{R}^2)}\right|^2. \tag{A.5}$$

Consider the inner integral

$$I(\rho) = \int_0^\infty \frac{\mathrm{d}a}{a^3} \left|\left\langle D_a^p \psi^p \middle| \Xi R_\rho^{-1}\phi\right\rangle_{L^2(\mathbb{R}^2)}\right|^2. \tag{A.6}$$

If ψ^p is an admissible wavelet on $L^2(\mathbb{R}^2)$, this integral converges, since $\Xi R_\rho^{-1}\phi \in L^2(\mathbb{R}^2)$ for any $\phi \in L^2(S^2)$.

In addition, for any $\phi \in L^2(S^2)$, $I(\rho)$ is a continuous function of $\rho \in \mathrm{SO}(3)$. The latter being compact, this function is bounded. Therefore,

$$I = \int_{\mathrm{SO}(3)} \mathrm{d}\nu(\rho)\, I(\rho) \tag{A.7}$$

also converges, again by the compactness of SO(3). This means that $\psi \in L^2(S^2)$ is an admissible spherical wavelet. □

Appendix B. Proof of Proposition 4.4

Let us define

$$S = \sum_{j\in\mathbb{Z}} \sum_{p,q\in\mathbb{Z}[2\beta_j]} v_j w_{jp} W_f(\omega_{jpq}, a_j) \overline{\widetilde{W}_f(\omega_{jpq}, a_j)}.$$

Since

$$W_f(\omega,a)=\sum_{(l,m)\in\mathcal{N}}\sqrt{\frac{4\pi}{2l+1}}\hat{f}(l,m)\overline{\hat{\psi}_a(l,0)}Y_l^m(\omega)$$

and

$$\widetilde{W}_f(\omega,a)=\sum_{(l,m)\in\mathcal{N}}\sqrt{\frac{4\pi}{2l+1}}G_\psi(l)^{-1}\hat{f}(l,m)\overline{\hat{\psi}_a(l,0)}Y_l^m(\omega),$$

we have

$$\begin{aligned}S&=\sum_{j\in\mathbb{N}}\sum_{p,q\in\mathbb{Z}[2\beta_j]}\sum_{(l,m)\in\mathcal{N}}\sum_{(l',m')\in\mathcal{N}}\frac{4\pi}{\sqrt{(2l+1)(2l'+1)}}\hat{f}(l,m)\overline{\hat{f}(l',m')}\\&\quad\times\nu_j w_{jp}G_\psi^{-1}(l)\overline{\hat{\psi}_{a_j}(l,0)}\hat{\psi}_{a_j}(l',0)Y_l^m(\omega_{jpq})\overline{Y_{l'}^{m'}(\omega_{jpq})}\\&=\sum_{j\in\mathbb{N}}4\pi\nu_j\sum_{(l,m)\in\mathcal{N}}\sum_{(l',m')\in\mathcal{N}}\frac{\hat{f}(l,m)\bar{\hat{f}}(l',m')}{\sqrt{(2l+1)(2l'+1)}}G_\psi^{-1}(l)\overline{\hat{\psi}_{a_j}(l,0)}\hat{\psi}_{a_j}(l',0)\\&\quad\times\sum_{p,q\in\mathbb{Z}[2\beta_j]}w_{jp}Y_l^k(\omega_{jpq})\overline{Y_{l'}^{k'}(\omega_{jpq})}.\end{aligned}$$

If $l+l'<\beta_j$, the product $Y_l^m\overline{Y_{l'}^{m'}}$ having order $l+l'$ [33], the weight w_{jp} provides the quadrature formula [8,12]

$$\sum_{p,q\in\mathbb{Z}[2\beta_j]}w_{jp}Y_l^m(\omega_{jpq})\overline{Y_{l'}^{m'}(\omega_{jpq})}=\int_{S^2}\mathrm{d}\mu(\omega)\,Y_l^m(\omega)\overline{Y_{l'}^{m'}(\omega)}=\delta_{ll'}\delta_{mm'},\tag{B.8}$$

for all $|m|\leqslant l$ and all $|m'|\leqslant l'$. Therefore, the sum S splits in two parts

$$S=\sum_{j\in\mathbb{N}}\sum_{p,q\in\mathbb{Z}[2\beta_j]}\sum_{\substack{(l,m)\in\mathcal{N}\\(l',m')\in\mathcal{N}\\l+l'<2\beta_j}}+\sum_{j\in\mathbb{N}}\sum_{p,q\in\mathbb{Z}[2\beta_j]}\sum_{\substack{(l,k)\in\mathcal{N}(l',m')\in\mathcal{N}\\l+l'\geqslant2\beta_j}}\ldots=C+D.$$

The first term C, where (B.8) is valid, reduces to

$$\begin{aligned}C&=\sum_{j\in\mathbb{N}}4\pi\nu_j\sum_{\substack{(l,m)\in\mathcal{N}\\l<\beta_j}}\frac{1}{(2l+1)}\big|\hat{f}(l,m)\big|^2G_\psi^{-1}(l)\big|\hat{\psi}_{a_j}(l,0)\big|^2\\&=\sum_{(l,m)\in\mathcal{N}}\big|\hat{f}(l,m)\big|^2\sum_{j\in\mathbb{N}}\frac{4\pi\nu_j}{(2l+1)}\mathbb{1}_{[0,\beta_j)}(l)G_\psi^{-1}(l)\big|\hat{\psi}_{a_j}(l,0)\big|^2.\end{aligned}$$

If (4.25) is verified, then

$$K_0\|f\|^2\leqslant C\leqslant K_1\|f\|^2.\tag{B.9}$$

Let us analyze the part D. Since $Y_l^m(\omega_{jpq})=Y_l^m(\theta_{jp},0)e^{\mathrm{i}m\varphi_{jq}}$, with $\theta_{jp}=\frac{2p+1}{4\beta_j}\pi$ and $\varphi_{jq}=\frac{q\pi}{\beta_j}$, we find

$$\sum_{q\in\mathbb{Z}[2\beta_j]} Y_l^m(\omega_{jpq})\overline{Y_{l'}^{m'}(\omega_{jpq})} = Y_l^m(\theta_{jp},0)\overline{Y_{l'm'}(\theta_{jp},0)} \sum_{q\in\mathbb{Z}[2\beta_j]} e^{\mathrm{i}(m-m')\frac{q\pi}{\beta_j}}$$
$$= 2\beta_j Y_l^m(\theta_{jp},0)\overline{Y_{l'}^{m'}(\theta_{jp},0)} \sum_{\substack{t\in\mathbb{Z}\\ |m+2t\beta_j|\leqslant l'}} \delta_{m',m+2t\beta_j}$$
$$= 2\beta_j \sum_{\substack{t\in\mathbb{Z}\\ |m+2t\beta_j|\leqslant l'}} Y_l^m(\theta_{jp},0)\overline{Y_{l'}^{m+2t\beta_j}(\theta_{jp},0)}\delta_{m',m+2t\beta_j}$$
$$= 2\beta_j \sum_{t\in\mathbb{Z}} \mathbb{1}_{[-l',l']}(m+2t\beta_j) Y_l^m(\theta_{jp},0)\overline{Y_{l'}^{m+2t\beta_j}(\theta_{jp},0)}\delta_{m',m+2t\beta_j}$$

So,

$$D = \sum_{j\in\mathbb{N}} 8\pi\nu_j\beta_j \sum_{(l,m)\in\mathcal{N}} \sum_{l'\in\mathbb{N}} \sum_{t\in\mathbb{Z}} \frac{\mathbb{1}_{[2\beta_j,\infty)}(l+l')\mathbb{1}_{[-l',l']}(m+2t\beta_j)}{\sqrt{(2l+1)(2l'+1)}} \hat{f}(l,m)\overline{\hat{f}(l',m+2t\beta_j)}$$
$$\times G_\psi^{-1}(l)\overline{\hat{\psi}}_{a_j}(l,0)\hat{\psi}_{a_j}(l',0) \sum_{p\in\mathbb{Z}[2\beta_j]} w_{jp} Y_l^m(\theta_{jp},0)\overline{Y_{l'}^{m+2t\beta_j}(\theta_{jp},0)}.$$

Therefore,

$$|D| \leqslant \sum_{j\in\mathbb{N}} 8\pi\nu_j\beta_j \sum_{(l,m)\in\mathcal{N}} \sum_{l'\in\mathbb{N}} \sum_{t\in\mathbb{Z}} \frac{\mathbb{1}_{[2\beta_j,\infty)}(l+l')\mathbb{1}_{[-l',l']}(m+2t\beta_j)}{\sqrt{(2l+1)(2l'+1)}} \big|\hat{f}(l,m)\big|\big|\hat{f}(l',m+2t\beta_j)\big|$$
$$\times G_\psi(l)^{-1}\big|\hat{\psi}_{a_j}(l,0)\big|\big|\hat{\psi}_{a_j}(l',0)\big| \sum_{p\in\mathbb{Z}[2\beta_j]} w_{jp}\big|Y_l^m(\theta_{jp},0)\big|\big|Y_{l'}^{m+2t\beta_j}(\theta_{jp},0)\big|$$
$$\leqslant \sum_{j\in\mathbb{N}} 4\pi\nu_j \sum_{(l,m)\in\mathcal{N}} \sum_{l'\in\mathbb{N}} \sum_{t\in\mathbb{Z}} \big|\hat{f}(l,m)\big|\big|\hat{f}(l',m+2t\beta_j)\big|\mathbb{1}_{[-l',l']}(m+2t\beta_j)$$
$$\times \mathbb{1}_{[\beta_j,\infty)}(l+l')G_\psi^{-1}(l)\big|\hat{\psi}_{a_j}(l,0)\big|\big|\hat{\psi}_{a_j}(l',0)\big|$$

where we used the fact that $|Y_l^m| \leqslant \sqrt{\frac{2l+1}{4\pi}}$ for all $(l,m)\in\mathcal{N}$, and $\sum_{p\in\mathbb{Z}[2\beta_j]} w_{jp} = \frac{4\pi}{2\beta_j}$.

The sums on m and t can be bounded since

$$\sum_{t\in\mathbb{Z}} \sum_{|m|\leqslant l} \big|\hat{f}(l,m)\big|\big|\hat{f}(l',m+2t\beta_j)\big|\mathbb{1}_{[-l',l']}(m+2t\beta_j)$$
$$\leqslant \sum_{t\in\mathbb{Z}} \Bigg[\sum_{|m|\leqslant l} \big|\hat{f}(l,m)\big|^2\mathbb{1}_{[-l',l']}(m+2t\beta_j)\Bigg]^{1/2} \Bigg[\sum_{|m|\leqslant l} \big|\hat{f}(l',m+2t\beta_j)\big|^2\mathbb{1}_{[-l',l']}(m+2t\beta_j)\Bigg]^{1/2}$$
$$\leqslant \Bigg[\sum_{t\in\mathbb{Z}} \sum_{|m|\leqslant l} \big|\hat{f}(l,m)\big|^2\mathbb{1}_{[-l',l']}(m+2t\beta_j)\Bigg]^{1/2} \Bigg[\sum_{t\in\mathbb{Z}} \sum_{|m|\leqslant l} \big|\hat{f}(l',m+2t\beta_j)\big|^2\mathbb{1}_{[-l',l']}(m+2t\beta_j)\Bigg]^{1/2}$$
$$\leqslant \Bigg[\sum_{|m|\leqslant l} \big|\hat{f}(l,m)\big|^2\Bigg[\frac{2l'+1}{2\beta_j}+1\Bigg]\Bigg]^{1/2} \Bigg[\sum_{t\in\mathbb{Z}} \sum_{m'=-l+2t\beta_j}^{l+2t\beta_j} \big|\hat{f}(l',m')\big|^2\mathbb{1}_{[-l',l']}(m')\Bigg]^{1/2}$$

$$
\begin{aligned}
&\leqslant \Bigg[\sum_{|m|\leqslant l} \big|\hat f(l,m)\big|^2\Big[\frac{2l'+1}{2\beta_j}+1\Big]\Bigg]^{1/2}\Bigg[\sum_{t\in\mathbb{Z}}\sum_{m'\in\mathbb{Z}} \big|\hat f(l',m')\big|^2 \mathbb{1}_{[-l,l]}(m'-2t\beta_j)\mathbb{1}_{[-l',l']}(m')\Bigg]^{1/2}\\
&\leqslant \Bigg[\sum_{|m|\leqslant l} \big|\hat f(l,m)\big|^2\Big[\frac{2l'+1}{2\beta_j}+1\Big]\Bigg]^{1/2}\Bigg[\sum_{t\in\mathbb{Z}}\sum_{m'=-l'}^{l'} \big|\hat f(l',m')\big|^2 \mathbb{1}_{[-l,l]}(m'-2t\beta_j)\Bigg]^{1/2}\\
&\leqslant \Bigg[\sum_{|m|\leqslant l} \big|\hat f(l,m)\big|^2\Big[\frac{2l'+1}{2\beta_j}+1\Big]\Bigg]^{1/2}\Bigg[\sum_{|m'|\leqslant l'} \big|\hat f(l',m')\big|^2\Big[\frac{2l+1}{2\beta_j}+1\Big]\Bigg]^{1/2}\\
&\leqslant (2\beta_j)^{-1}\big(2(l+\beta_j)+1\big)^{1/2}\big(2(l'+\beta_j)+1\big)^{1/2}\Bigg[\sum_{|m|\leqslant l} \big|\hat f(l,m)\big|^2\Bigg]^{1/2}\Bigg[\sum_{|m'|\leqslant l'} \big|\hat f(l',m')\big|^2\Bigg]^{1/2},
\end{aligned}
$$

applying the Cauchy–Schwarz inequality first on the sum over m and then on the sum over t. Therefore,

$$
|D| \leqslant \sum_{l,l'\in\mathbb{N}}\Bigg[\sum_{|m|\leqslant l} \big|\hat f(l,m)\big|^2\Bigg]^{1/2}\Bigg[\sum_{|m'|\leqslant l'} \big|\hat f(l',m')\big|^2\Bigg]^{1/2}\chi(l,l')
$$

with

$$
\chi(l,l') = \sum_{j\in\mathbb{N}} \frac{2\pi\nu_j c_j(l,l')}{\beta_j}\mathbb{1}_{[2\beta_j,\infty)}(l+l')G_\psi^{-1}(l)\big|\hat\psi_{a_j}(l,0)\big|\big|\hat\psi_{a_j}(l',0)\big|.
$$

and $c_j(l,l') = (2(l+\beta_j)+1)^{\frac12}(2(l'+\beta_j)+1)^{\frac12}$.

Introducing $F_l^2 = \sum_{|m|\leqslant l} |\hat f(l,m)|^2$, we obtain with the Cauchy–Schwarz inequality

$$
|D| \leqslant \sum_{l\in\mathbb{N}} F_l \sum_{l'\in\mathbb{N}} \chi(l,l')F_{l'} \leqslant \|F\|\|\mathcal{X}F\| = \|f\|\|\mathcal{X}F\|,
$$

with $F = (F_l)_{l\in\mathbb{N}}$, $\|F\|^2 = \sum_{l\in\mathbb{N}} |F_l|^2 = \|f\|^2$, $\mathcal{X} = \big(\chi(l,l')\big)_{l,l'\in\mathbb{N}}$, and $(\mathcal{X}F)_l = \sum_{l'\in\mathbb{N}} \chi(l,l')F_{l'}$. If (4.25) is satisfied, we have

$$
|D| \leqslant \|f\|\|\mathcal{X}\|\|f\| = \delta\|f\|^2,
$$

with the norm

$$
\|\mathcal{X}\| = \sup_{(G_l)_{l\in\mathbb{N}}} \frac{\|\mathcal{X}G\|}{\|G\|}.
$$

The proof of the theorem is provided by noting that

$$
0 < (K_0-\delta)\|f\|^2 < C - |D| \leqslant S \leqslant C + |D| < (K_1+\delta)\|f\|^2 < \infty. \qquad \square
$$

References

[1] E.H. Adelson, J.R. Bergen, The plenoptic function and the elements of early vision, in: M. Landy, J.A. Movshon (Eds.), Computational Models of Visual Processing, MIT Press, Cambridge, MA, 1991.

[2] S.T. Ali, J-P. Antoine, J-P. Gazeau, Continuous frames in Hilbert space, Ann. Phys. 222 (1993) 1–37.

[3] S.T. Ali, J-P. Antoine, J-P. Gazeau, Coherent States, Wavelets, and Their Generalizations, Springer-Verlag, New York, 2000.

[4] J-P. Antoine, P. Vandergheynst, Wavelets on the 2-sphere: A group theoretical approach, Appl. Comput. Harmon. Anal. 7 (1999) 1–30.
[5] J-P. Antoine, L. Demanet, L. Jacques, P. Vandergheynst, Wavelets on the sphere: Implementation and approximations, Appl. Comput. Harmon. Anal. 13 (2002) 177–200.
[6] J-P. Antoine, A.L. Hohouéto, Discrete frames of Poincaré coherent states in $1 + 3$ dimensions, J. Fourier Anal. Appl. 9 (2003) 141–173.
[7] J-P. Antoine, R. Murenzi, P. Vandergheynst, S.T. Ali, Two-Dimensional Wavelets and Their Relatives, Cambridge Univ. Press, Cambridge, UK, 2004.
[8] J. Boyd, Chebyshev and Fourier Spectral Methods, Lecture Notes in Engineering, vol. 49, Springer-Verlag, New York, 1989.
[9] T. Bülow, Multiscale image processing on the sphere, in: Proc. 24th DAGM-Symposium, in: Lecture Notes in Comput. Sci., vol. 2449, Springer-Verlag, London, UK, 2002, pp. 609–617.
[10] M. Cruz, E. Martinez-Gonzalez, P. Vielva, L. Cayon, Detection of a non-Gaussian spot in WMAP, Mon. Not. R. Astron. Soc. 356 (2005) 29–40.
[11] I. Daubechies, Ten Lectures on Wavelets, SIAM, Philadelphia, PA, 1992.
[12] J.R. Driscoll, D.M. Healy, Computing Fourier transforms and convolutions on the 2-sphere, Adv. in Appl. Math. 15 (1994) 202–250.
[13] R.J. Duffin, A.C. Schaeffer, A class of nonharmonic Fourier series, Trans. Amer. Math. Soc. 72 (1952) 341–366.
[14] W. Freeden, T. Maier, S. Zimmermann, A survey on wavelet methods for (geo)applications, Rev. Math. Complut. 16 (1) (2003).
[15] GNU General Public License, http://www.gnu.org/copyleft/gpl.html.
[16] M. Holschneider, Continuous wavelet transforms on the sphere, J. Math. Phys. 37 (1996) 4156–4165.
[17] L. Jacques, Ondelettes, repères et couronne solaire, Thèse de doctorat, Université catholique de Louvain, Louvain-la-Neuve, Belgium, 2004.
[18] R. Kronland-Martinet, Private communication.
[19] S. Mallat, A Wavelet Tour of Signal Processing, second ed., Academic Press, San Diego, CA, 1999.
[20] N.L. Max, E.D. Getzoff, Spherical harmonic molecular surfaces, IEEE Comput. Graph. Appl. 8 (1988) 42–50.
[21] J.D. McEwen, M.P. Hobson, A.N. Lasenby, D.J. Mortlock, A high-significance detection of non-Gaussianity in the WMAP 1-year data using directional spherical wavelets, Mon. Not. R. Astron. Soc. 359 (2005) 1583–1596.
[22] H.N. Mhaskar, F.J. Narcowich, J. Prestin, J.D. Ward, Polynomial frames on the sphere, Adv. Comput. Math. 13 (2000) 387–403.
[23] E. Praun, H. Hoppe, Spherical parametrization and remeshing, ACM Trans. Graph. 22 (3) (2003) 340–349.
[24] D. Rockmore, S. Moore, D. Healy, P. Kostelec, SpharmonicKit is a freely available collection of C programs for doing Legendre and scalar spherical transforms developed at Dartmouth College, available at: http://www.cs.dartmouth.edu/~geelong/sphere/.
[25] B. Rubin, Continuous wavelet transforms on a sphere, in: Y.Y. Zeevi, R. Coifman (Eds.), Signal and Image Representation in Combined Spaces, Academic Press, San Diego, 1998, pp. 457–476.
[26] B. Rubin, Spherical Radon transform and related wavelet transforms, Appl. Comput. Harmon. Anal. 5 (1998) 202–215.
[27] P. Schröder, W. Sweldens, Spherical wavelets: Efficiently representing functions on the sphere, Comput. Graph. 29 (1995) 161–172.
[28] B. Torrésani, Position–frequency analysis for signals defined on spheres, Signal Proc. 43 (1995) 341–346.
[29] B. Torrésani, Analyse continue par ondelettes, InterEditions/CNRS Editions, Paris, 1995.
[30] I. Tosic, I. Bogdanova, P. Frossard, P. Vandergheynst, Multiresolution motion estimation for omnidirectional images, in: Proc. EUSIPCO, 2005, in press.
[31] J. Turski, Projective Fourier analysis for patterns, Pattern Recognition 33 (12) (2000) 2033–2043.
[32] J. Turski, Geometric Fourier analysis of the conformal camera for active vision, SIAM Rev. 46 (2) (2003) 230–255.
[33] N.J. Vilenkine, Fonctions spéciales et théorie de la représentation des groupes, Dunod, Paris, 1969.
[34] Y. Wiaux, L. Jacques, P. Vandergheynst, Correspondence principle between spherical and Euclidean wavelets, Astrophys. J. (2005), in press.